frontiers in Cellular Neuroscience

ORIGINAL RESEARCH
published: 25 June 2020
doi: 10.3389/fncel.2020.00160

Small-Medium Extracellular Vesicles and Their miRNA Cargo in Retinal Health and Degeneration: Mediators of Homeostasis, and Vehicles for Targeted Gene Therapy

Yvette Wooff[1,2†], Adrian V. Cioanca[1†], Joshua A. Chu-Tan[1,2], Riemke Aggio-Bruce[1,2], Ulrike Schumann[1] and Riccardo Natoli[1,2]*

[1] The John Curtin School of Medical Research, The Australian National University, Canberra, ACT, Australia, [2] The ANU Medical School, The Australian National University, Canberra, ACT, Australia

OPEN ACCESS

Edited by:
Raymond Ching-Bong Wong, Centre for Eye Research Australia, Australia

Reviewed by:
Tadao Maeda, Kobe City Medical Center General Hospital, Japan
Natalia Martinez-Gil, University of Alicante, Spain

***Correspondence:**
Riccardo Natoli
riccardo.natoli@anu.edu.au

[†] These authors have contributed equally to this work

Specialty section:
This article was submitted to Cellular Neuropathology, a section of the journal Frontiers in Cellular Neuroscience

Received: 28 March 2020
Accepted: 13 May 2020
Published: 25 June 2020

Citation:
Wooff Y, Cioanca AV, Chu-Tan JA, Aggio-Bruce R, Schumann U and Natoli R (2020) Small-Medium Extracellular Vesicles and Their miRNA Cargo in Retinal Health and Degeneration: Mediators of Homeostasis, and Vehicles for Targeted Gene Therapy. Front. Cell. Neurosci. 14:160. doi: 10.3389/fncel.2020.00160

Photoreceptor cell death and inflammation are known to occur progressively in retinal degenerative diseases such as age-related macular degeneration (AMD). However, the molecular mechanisms underlying these biological processes are largely unknown. Extracellular vesicles (EV) are essential mediators of cell-to-cell communication with emerging roles in the modulation of immune responses. EVs, including exosomes, encapsulate and transfer microRNA (miRNA) to recipient cells and in this way can modulate the environment of recipient cells. Dysregulation of EVs however is correlated to a loss of cellular homeostasis and increased inflammation. In this work we investigated the role of isolated retinal small-medium sized EV (s-mEV) which includes exosomes in both the healthy and degenerating retina. Isolated s-mEV from normal retinas were characterized using dynamic light scattering, transmission electron microscopy and western blotting, and quantified across 5 days of photo-oxidative damage-induced degeneration using nanotracking analysis. Small RNAseq was used to characterize the miRNA cargo of retinal s-mEV isolated from healthy and damaged retinas. Finally, the effect of exosome inhibition on cell-to-cell miRNA transfer and immune modulation was conducted using systemic daily administration of exosome inhibitor GW4869 and *in situ* hybridization of s-mEV-abundant miRNA, miR-124-3p. Electroretinography and immunohistochemistry was performed to assess functional and morphological changes to the retina as a result of GW4869-induced exosome depletion. Results demonstrated an inverse correlation between s-mEV concentration and photoreceptor survivability, with a decrease in s-mEV numbers following degeneration. Small RNAseq revealed that s-mEVs contained uniquely enriched miRNAs in comparison to in whole retinal tissue, however, there was no differential change in the s-mEV miRNAnome following photo-oxidative damage. Exosome inhibition via the use of GW4869 was also found to exacerbate retinal degeneration, with reduced retinal function and increased levels of inflammation and cell death demonstrated following photo-oxidative damage in exosome-inhibited mice. Further, GW4869-treated

mice displayed impaired translocation of photoreceptor-derived miR-124-3p to the inner retina during damage. Taken together, we propose that retinal s-mEV and their miRNA cargo play an essential role in maintaining retinal homeostasis through immune-modulation, and have the potential to be used in targeted gene therapy for retinal degenerative diseases.

Keywords: retina, neurodegeneration, extracellular vesicle, microRNA, immuno-modulation, gene therapy

INTRODUCTION

Retinal degenerative diseases comprise a heterogeneous group of visual disorders associated with neuroinflammation and the progressive death of retinal neurons, often resulting in irreversible blindness (Ratnapriya and Swaroop, 2013). Despite advances in understanding the pathogenesis and progression of retinal degenerative diseases (Donoso et al., 2006; Janik-Papis et al., 2009; Knickelbein et al., 2015), the precise molecular mechanisms that propagate retinal inflammation and subsequent cell death remain unknown. The study of extracellular vesicles (EV), including exosomes, might provide greater clarity in unpicking these mechanisms given their role as endogenous modulators of biological processes, including in inflammation (Chan et al., 2019), and intracellular communication pathways (Yuana et al., 2013; Isola and Chen, 2017; Mathieu et al., 2019).

Extracellular vesicle are small membrane-enclosed delivery vehicles which have been widely investigated for their vital role in mediating cell-to-cell communication in both healthy as well as diseased states (Yuana et al., 2013; Isola and Chen, 2017; Mathieu et al., 2019). Exosomes, the smallest EV fraction (40–200 nm in diameter) (Théry et al., 2002; Vella et al., 2017; Hessvik and Llorente, 2018; Słomka et al., 2018), in particular, have recently been implicated in the pathogenesis of retinal degenerative diseases. These include Age-Related Macular Degeneration (AMD) (Wang et al., 2009; Klingeborn et al., 2017; Hsu et al., 2018; Li et al., 2019), Diabetic Retinopathy (Huang et al., 2018), and Retinitis Pigmentosa (Vidal-Gil et al., 2019).

Exosomes are released by nearly all cell types and are formed via the endocytic pathway, with the invagination of the endosomal membrane allowing intraluminal vesicle formation in multivesicular bodies (MVB) (Van Niel et al., 2006). Biogenesis occurs either in an endosomal sorting complex required for transport (ESCRT)-dependent or ESCRT-independent manner (Kowal et al., 2014; Li et al., 2019), the latter of which can be blocked using GW4869, a non-competitive inhibitor of neutral sphingomyelinase 2 (nSMase2) – the key enzyme for generating exosomes via the ESCRT-independent pathway (Luberto et al., 2002). Following biogenesis, the MVB fuses with the host cell plasma membrane and releases the internalized exosomes into the extracellular environment (Van Niel et al., 2006; Abels and Breakefield, 2016; Hessvik and Llorente, 2018). From here, exosomes can travel to nearby or distant target cells, often through biological fluids such as blood (Charlotte et al., 2016), to exert their biological effects (Van der Pol et al., 2012; Yáñez-Mó et al., 2015; Abels and Breakefield, 2016). As exosomes selectively incorporate proteins, mRNA and non-coding RNA such as microRNA (miRNA) from their host cell (reviewed in Yáñez-Mó et al., 2015; Abels and Breakefield, 2016), the transfer of exosomal contents can alter the environment of target recipient cells. In a healthy state, the transfer of exosomal nucleic acid contents, including miRNA, is required for homeostatic maintenance (Desdín-Micó and Mittelbrunn, 2017; Fleshner and Crane, 2017). However, in disease, aberrations to this process or the selective encapsulation of toxic proteins and/or dysregulated miRNA, can cause progressive inflammation (Gupta and Pulliam, 2014; Alexander et al., 2015).

miRNA have been labeled as 'master regulators' of gene expression, due to their ability to target and repress multiple genes within and across different biological pathways (Christopher et al., 2016). This regulatory power makes them ideal therapeutic and diagnostic molecules (Rupaimoole and Slack, 2017), in particular to combat dysregulated immune responses, such as those occurring in retinal degenerations (Bartel, 2009; Christopher et al., 2016). miRNA have been reported to be enriched in exosomes over their host cells, suggesting that they are selectively incorporated to serve a dynamic, fast-response biological need (Squadrito et al., 2014; Bhome et al., 2018).

The biological importance of exosomes and exosomal-miRNA (exoMiR) is reflected by their association with a range of inflammatory (Van Hezel et al., 2017; Cypryk et al., 2018), autoimmune (Long et al., 2018; Anel et al., 2019) and neurodegenerative diseases (Jan et al., 2017; Soria et al., 2017; Jain et al., 2019). These include diabetes (Saeedi et al., 2018), rheumatoid arthritis (Skriner et al., 2006; Zhang et al., 2006; Wan et al., 2019), and Alzheimer's and Parkinson's disease (Gupta and Pulliam, 2014; Li et al., 2018; Jain et al., 2019; Sackmann et al., 2019). exoMiR have been reported to play pathogenic roles in these diseases by promoting angiogenesis (Kosaka et al., 2013; Atienzar−Aroca et al., 2016), and modulating immune responses, including in the recruitment of immune cells (Théry et al., 2002; Abusamra et al., 2005; Robbins and Morelli, 2014; Ye et al., 2014; Wong et al., 2016; Van Hezel et al., 2017); features that contribute to cell death. To date however, the identification and role of exosomes and their miRNA cargo in the retina in both healthy and diseased states, is largely unexplored (Klingeborn et al., 2017; Li et al., 2019). While small EV fractions isolated following high speed $> 100{,}000 \times g$ ultracentrifugation and expressing tetraspanin markers CD9, CD63, and CD81 (such as those isolated in this work) are commonly referred to as exosomes, without evidence of endosomal origin and in complying with

MISEV 2018 guidelines (Théry et al., 2018), are herein referred to as small-to-medium EV, or s-mEV. In reference to other works, EV terminology will be referred to as published in the original papers.

Characterizing the role of s-mEV and their miRNA cargo in both the normal and degenerating retina will aid in elucidating novel cell-to-cell communication pathways that could play a role in propagating inflammation during retinal degenerative diseases. Furthermore, uncovering the miRNA signature within retinal s-mEV as well as their potential binding partners may reveal novel regulatory mechanisms underpinning retinal degenerations, ultimately leading to the discovery of therapeutic targets. This study characterizes for the first time, retinal-derived s-mEV from both the healthy and degenerating mouse retina using a previously established model of photo-oxidative damage-induced retinal degeneration (Natoli et al., 2016). Photo-oxidative damage models such as the one employed in this study accurately replicate key pathological changes seen in AMD, including the upregulation of oxidative stress and inflammatory pathways, progressive centralized focal photoreceptor cell loss and microglial/macrophage recruitment and activation (Marc et al., 2008; Tanito et al., 2008; Natoli et al., 2016; Abokyi et al., 2020).

We show that s-mEV secretion is inversely correlated to photoreceptor survivability, with the severity of retinal degeneration directly correlating to decreased retinal s-mEV numbers. We used small RNAseq to characterize the miRNA cargo of retinal s-mEV (exoMiR). Although we demonstrated that there was no change in s-mEV miRNA-cargo in response to retinal degeneration, we found that s-mEVs contain a set of uniquely enriched miRNAs. Further, we show that miRNA contained in retinal s-mEV were associated with the regulation of inflammatory, cell survival and motility pathways. Upon systemic exosome inhibition using GW4869, retinal function in healthy and photo-oxidative damaged mice was significantly reduced compared to controls. In addition, photoreceptor cell death and inflammation were significantly increased in GW4869-injected photo-oxidative damaged mice, compared to controls. Using *in situ* hybridization, we further demonstrated that the expression of miR-124-3p in the inner retina was reduced in GW4869-injected photo-oxidative damaged mice, suggesting that miR-124-3p movement could be mediated through s-mEV-dependent transport.

Taken together, these results suggest a novel role for s-mEV and s-mEV-miRNA-mediated cell-to-cell communication in the retina. We demonstrate that maintaining and transporting necessary levels of s-mEV cargo is required for normal retinal homeostasis and immunomodulation, with insufficient bioavailability of s-mEV potentially leading to inflammatory cell death (see **Figure 10**). In addition, this work elucidates downstream biological targets of s-mEV-miRNA that are required for retinal homeostatic maintenance, and identifies potential miRNA and mRNA therapeutic targets for further investigations.

MATERIALS AND METHODS

Animal Handling and Photo-Oxidative Damage

All experiments were conducted in accordance with the ARVO Statement for the Use of Animals in Ophthalmic and Vision Research and with approval from the Australian National University's (ANU) Animal Experimentation Ethics Committee (AEEC) (Ethics ID: A2017/41; Rodent models and treatments for retinal degenerations). Adult male and female C57BL/6J wild-type (WT) mice (aged between 50 and 90 postnatal days) were bred and reared under 12 h light/dark cycle conditions (5 lux) with free access to food and water. The C57BL/6J colony was genotyped for the presence of both the $Rpe65^{450Met}$ polymorphism or the deleterious $Crb1^{rd8}$ mutation using previously published primer sets (Kim et al., 2004; Mattapallil et al., 2012). Sequencing for these was conducted at the ACRF Biomolecular Resource Facility, ANU. All animals used possessed the $Rpe65^{450Met}$ polymorphism but were free of the $Crb1^{rd8}$ mutation. Littermate age-matched WT mice were randomly assigned to photo-oxidative damage (PD) and dim-reared control (DR) groups. Animals in the photo-oxidative damage group were continuously exposed to 100k lux white LED light for a period of 1, 3, or 5 days as described previously (Natoli et al., 2016), with the majority of experiments conducted for 5 days. Dim-reared control mice were maintained in 12 h light (5 lux)/dark cycle conditions.

Retinal s-mEV Isolation

Mice were euthanized with CO_2 following experimental runs. Either two (from one mouse) or four (from two mice – used for high-throughput sequencing) retinas were pooled and collected in Hanks Buffered Saline Solution (HBSS, Gibco; Thermo Fisher Scientific, MA, United States). Retinas were transferred to 500 μL digestion solution [(HBSS containing 2.5 mg/mL papain (Worthington Biochemical, NJ, United States), 200U DNase I (Roche Diagnostics, NSW, Australia), 5 μg/mL catalase (Sigma-Aldrich, MO, United States), 10 μg/mL gentamycin (Sigma-Aldrich, MO, United States) and 5 μg/mL superoxide dismutase (Worthington Biochemical, NJ, United States)] and finely chopped using scissors. Retinas were incubated at 37°C for 8 min, followed by 20 min at 8°C, to allow for the breakdown of the extracellular matrix and s-mEV release. Following digestion, tissue suspensions were neutralized by diluting in 11.5 mL of HBSS and centrifuged at 1000 × *g* for 10 minutes at 4°C to remove cells and cell debris. The supernatant was transferred to 14 × 89 mm Beckman Ultra-Clear ultracentrifuge tubes (Beckman Coulter, CA United States) and centrifuged at 10,000 × *g* for 30 min at 4°C in a Beckman Coulter Optima XE-100 [fitted with a SW41Ti Rotor (Beckman Coulter, CA, United States)], to collect large EVs and remaining cell debris. The s-mEV-containing supernatant was transferred to new ultracentrifuge tubes and centrifuged for

1.5 h at 150,000 × *g* at 4°C. The supernatant was carefully decanted, and the s-mEV pellet resuspended via tituration for 1 min in 500 μL Ultrapure Endotoxin-free 0.1M PBS (Thermo Fisher Scientific, MA, United States) and used immediately for quantification.

For RNA isolation, the s-mEV pellet was resuspended immediately in 100 μl RNAse A (10 μg/ml in Ultrapure Endotoxin-free 0.1M PBS) and incubated for 30 minutes at 37°C to digest any RNA contamination. Following RNase treatment, s-mEV RNA was extracted using the mirVana miRNA Isolation Kit (Thermo Fisher Scientific, MA, United States) as per section "RNA Extraction."

S-mEV Characterization

NanoSight

The size and concentration of s-mEV were measured using nanoparticle tracking analysis on a NanoSight NS300 (Malvern Instruments, Malvern, United Kingdom). s-mEV samples were diluted 1:20 (retinal s-mEV) or 1:40 (cell culture s-mEV) in 1 ml Ultrapure Endotoxin-free 0.1M PBS to achieve a particle per frame value between 20 and 100. Samples were analyzed under constant flow provided by a syringe pump set at a speed of 35 (equating to ∼3.1 μl/min; Gerritzen et al., 2017). A total of nine 30 s long videos were captured (camera setting: 14) for each sample. The detection threshold was set between 4 and 5 and was not altered between measurements of the same experiment. The concentration values, modal and mean sizes were exported to Prism V7 (GraphPad Software, CA, United States) for statistical analysis and plotting.

Zetasizer

Dynamic light scattering measurements were performed using a Zetasizer Nano ZS 90 (Malvern Instruments, Malvern, United Kingdom). A 500 μL undiluted retinal s-mEV suspension in Ultrapure Endotoxin-free 0.1M PBS was prepared, loaded in a low-volume disposable sizing cuvette (ZEN0112, Malvern Instruments, Malvern, United Kingdom) and agitated before measurements. Measurement parameters were set as follows: Material Refractive Index – 1.46, Dispersant Refractive Index – 1.330, Viscosity (cP) – 0.888, Temperature (°C) – 25, and Measurement Duration (s) – 60. The acquired intensity data was transformed using the General-Purpose Model within the Zetasizer analysis software to generate the size distribution of the s-mEV.

Transmission Electron Microscopy (TEM)

A 30 μl retinal s-mEV suspension was placed on a 200-mesh carbon-coated copper grid (Sigma-Aldrich, MO, United States) pre-treated with glow discharge using an Emtech K100X system (Quorum Technologies, Sussex, United Kingdom). After 20 min, s-mEV were contrasted with 2% uranyl acetate solution for 1 minute, followed by three washes in 0.22 μm filtered PBS (Thermo Fisher Scientific, MA, United States). Excess PBS was removed by placing a piece of absorbent paper at the edge of the grid. The grids were imaged on a Hitachi 7100 FA transmission electron microscope (Hitachi, Tokyo, Japan) at 100 kV. The images were captured with a side mounted Gatan Orius CCD camera (Gatan, CA, United States) at 4008 × 2672 pixels resolution using a 2 s exposure operated through Gatan Microscopy Suite (Gatan, CA, United States). A total of 20 images were captured at 100,000x magnification from four different grids, each containing s-mEV isolated from a different retinal s-mEV preparation (2 mouse retinas/preparation). The images were imported into ImageJ V2.0 software (National Institutes of Health, Bethesda, MD, United States), scale-calibrated and the diameter of approximately 230 s-mEV was measured. The size distribution was plotted in a histogram with 20 nm wide bins using Prism V7.0 (GraphPad Software, CA, United States).

Western Blot

s-mEV pellets (see section "Retinal s-mEV Isolation") were immediately lysed in 50 μL CellLyticTM Cell Lysis Buffer (supplemented with 1:100 protease inhibitor cocktail; Sigma-Aldrich, MO, United States). The blot was performed as previously described (Jiao et al., 2018). Briefly, 10 μg of denatured protein was loaded onto Novex 4-20% Tris-Glycine Mini Gels (Thermo Fisher Scientific, MA, United States) and subjected to electrophoresis (45 min, 150 V). The protein bands were transferred (45 min, 20 V) to a nitrocellulose membrane (Bio-Rad, CA, United States) using the Power Blotter semi-dry system (Thermo Fisher Scientific, MA, United States). Membranes were then washed in PBS-Tween (0.025%; PBS-T), blocked in 3% BSA for 1 h and then incubated overnight at 4°C with primary s-mEV marker antibodies CD63 (1:1000, Ts63, Thermo Fisher Scientific, MA, United States), CD81 (1:2000, ab109201, Abcam, Cambridge, United Kingdom) or CD9 (1:2000, ab92726, Abcam, Cambridge, United Kingdom). Following three washes in PBS-T, blots were incubated in appropriate secondary antibodies, HRP-conjugated Goat Anti-Rabbit IgG (H + L) (1:1000, 170-6515, Bio-Rad, CA, United States) or Goat-anti-Mouse IgG (1:1000, 170-6516, Bio-Rad, CA, United States) for 2 h at room temperature. Membranes were washed in PBS-T and developed for 2 min with Clarity™ Western ECL Substrate (Bio-Rad, CA, United States). Imaging was performed using a ChemiDoc™ MP Imaging System with Image Lab™ software (Bio-Rad, CA, United States).

Exosome Inhibition

Exosome inhibition was performed using GW4869 (Sigma-Aldrich, MO, United States), a known inhibitor of exosome biogenesis and release (Catalano and O'Driscoll, 2020). GW4869 was reconstituted in dimethyl sulfoxide (DMSO; Sigma-Aldrich, MO, United States) to a concentration of 5 mM and used as a stock solution for further dilution in Ultrapure Endotoxin-free 0.1M PBS. Mice were injected with 1.25 mg/kg GW4869 via intraperitoneal (I.P.) injection daily for 5 days. 10.3% DMSO in Ultrapure Endotoxin-free 0.1M PBS (corresponding to the final volume of DMSO in GW4869 preparations) was used as a negative control. All mice were monitored daily for signs of distress or sickness.

Retinal Assessment

Retinal Function via Electroretinography (ERG)

To assess retinal function full-field scotopic ERG was performed as previously described (Natoli et al., 2017). Briefly, mice were dark-adapted overnight before being anesthetized with an intraperitoneal injection of Ketamine (100 mg/kg; Troy Laboratories, NSW, Australia) and Xylazil (10 mg/kg; Troy Laboratories, NSW, Australia). Both pupils were dilated with one drop each of 2.5% w/v Phenylephrine hydrochloride and 1% w/v Tropicamide (Bausch and Lomb, NY, United States).

Anesthetized and pupil dilated mice were placed on the thermally regulated stage of the Celeris ERG system (Diagnosys LLC, MA, United States). The Celeris ERG system has combined Ag/AgCl electrode-stimulator eye probes which measure the response from both eyes simultaneously, and uses 32-bit ultra-low noise amplifiers fitted with impedance testing. Eye probes were cleaned with 70% ethanol and then a 0.3% Hypromellose eye drop solution (GenTeal; Novartis, NSW, Australia) was applied to both probes. The probes were then placed covering and just touching the surface of each eye. A single- or twin-flash paradigm was used to elicit a mixed response from rods and cones. Flash stimuli for mixed responses were provided using 6500K white flash luminance range over stimulus intensities from -0.01 – 40 log.cd.s.m^{-2}. Responses were recorded and analyzed using Espion V6 Software (Diagnosys LLC, MA, United States). Statistics were performed in Prism V7.0 using a two-way analysis of variance (ANOVA) to test for differences in a-wave and b-wave responses. Data was expressed as the mean wave amplitude ± SEM (μV).

Optical Coherence Tomography (OCT)

Cross-sectional images of live mouse retinas were taken at 1 mm increments from the optic nerve using a Spectralis HRA + OCT device (Heidelberg Engineering, Heidelberg, Germany) as previously described (Natoli et al., 2016). Eye gel (GenTeal; Novartis, NSW, Australia) was administered to both eyes for recovery.

Using OCT cross-sectional retinal images, and ImageJ V2.0 software (National Institutes of Health, Bethesda, MD, United States), the thickness of the outer nuclear layer (ONL), was calculated as the ratio to the whole retinal thickness (outer limiting membrane to the inner limiting membrane).

Retinal Tissue Collection and Preparation

Animals were euthanized with CO_2 following functional ERG analysis. The superior surface of the left eye was marked and enucleated, then immersed in 4% paraformaldehyde for 3 h. Eyes were then cryopreserved in 15% sucrose solution overnight, embedded in OCT medium (Tissue Tek, Sakura, Japan) and cryosectioned at 12 μm in a parasagittal plane (superior to inferior) using a CM 1850 Cryostat (Leica Biosystems, Germany). To ensure accurate comparisons were made for histological analysis, only sections containing the optic nerve head were used for analysis. The retina from the right eye was excised through a corneal incision and placed into RNAlater solution (Thermo Fisher Scientific, MA, United States) at 4°C overnight and then stored at −80°C until further use.

Immunolabeling

Immunohistochemical analysis of retinal cryosections was performed as previously described (Rutar et al., 2015). Fluorescence was visualized and images taken using a laser-scanning A1$^+$ confocal microscope at 20x magnification (Nikon, Tokyo, Japan). Images panels were analyzed using ImageJ V2.0 software and assembled using Photoshop CS6 software (Adobe Systems, CA, United States).

IBA-1 Immunohistochemistry

Immunolabeling for IBA-1 (1:500, 019-19741, Wako, Osaka, Japan) and quantification was performed as previously described (Rutar et al., 2015). The number of IBA-1$^+$ cells (a marker of retinal microglia and macrophages) was counted across the superior and inferior retina using two retinal sections per mouse and then averaged. Retinal cryosections were stained with the DNA-specific dye bisbenzimide (1:10000, Sigma-Aldrich, MO, United States) to visualize the cellular layers.

TUNEL Assay

Terminal deoxynucleotidyl transferase (Tdt) dUTP nick end labeling (TUNEL), was used as a measure of photoreceptor cell death. TUNEL *in situ* labeling was performed on retinal cryosections using a Tdt enzyme (Cat# 3333566001, Sigma-Aldrich, MO, United States) and biotinylated deoxyuridine triphosphate (dUTP) (Cat# 11093070910, Sigma-Aldrich, MO, United States) as previously described (Natoli et al., 2010). Images of TUNEL staining were captured with the A1$^+$ Nikon confocal microscope at 20x magnification. The total number of TUNEL$^+$ cells were counted including both the superior and inferior retina using two retinal sections per animal, and is represented as the average number of TUNEL$^+$ cells per retinal section.

To further quantify photoreceptor survival, the thickness of the ONL on retinal cryosections was determined by counting the number of nuclei rows (photoreceptor cell bodies) in the area of retinal lesion development (1 mm superior to the optic nerve head). Photoreceptor cell row quantification was performed five times per retina using two retinal cryosections at comparable locations per mouse. The thickness the ONL, inner nuclear layer (INL), and the combined ganglion cell layer (GCL)-outer plexiform layer (OPL) thickness were also measured at the lesion site on the superior retina, and expressed as a ratio to whole retinal thickness.

In situ Hybridization

Localization of miR-124-3p within the retina was determined by *in situ* hybridization. A double DIG-labeled miR-124-3p miRCURY LNA miRNA Detection Probe (Exiqon, Vedbaek, Denmark) was used on retinal cryosections, which were hybridized for 1 h at 53°C as previously described (Chu-Tan et al., 2018). The bound probe was visualized using 5-bromo-4-chloro-3 indoyl phosphate (NBT/BCIP; Sigma-Aldrich Corp., St. Louis, MO, United States). Bright field images were captured on the A1$^+$ Nikon confocal microscope fitted with a DS-Ri1-U3 color camera

at 20x magnification and 4076 × 3116 pixel resolution. All images were centered at the site of lesion located approximately 1mm superiorly to the optic nerve head. The images were imported into ImageJ V2.0 software, converted to 8-bit format and then the densitometry was calculated. Mean gray values were measured at five different locations along the INL, ONL and the outer limiting membrane/photoreceptor inner segment region with background levels subtracted prior.

RNA Extraction

RNA (enriched for miRNA) extraction and purification from retinas or RNase A treated s-mEV pellets was performed using an acid-phenol:chloroform extraction method with the mirVana miRNA Isolation Kit (Thermo Fisher Scientific, MA, United States) according to the manufacturer's instructions. The concentration and purity of each RNA sample was assessed using the ND-1000 spectrophotometer (Nanodrop Technologies, DE, United States). The size distribution and concentration of s-mEV miRNA was further assessed using a 2100 Agilent Bioanalyzer with an Agilent Small RNA Kit (Agilent Technologies, CA, United States), according to the manufacturers' instruction.

cDNA Synthesis From mRNA and miRNA Templates

Following purification of RNA, cDNA was synthesized from 1 μg RNA using either the Tetro cDNA Synthesis Kit (Bioline Reagents, London, United Kingdom) from an mRNA template, or using the TaqMan MicroRNA RT kit (Thermo Fisher Scientific) from a miRNA template, according to manufacturers' instructions.

Quantitative Real-Time Polymerase Chain Reaction

The expression of ESCRT-independent exosome biogenesis pathways genes was measured by qRT-PCR. We targeted *Pdcd6ip* (also known as *Alix*), which encodes an accessory protein in the ESCRT-dependent pathway, and *Smpd3*, which encodes nSMase2 in the ESCRT-independent pathway (Hessvik and Llorente, 2018). The expression of miR-124-3p was also investigated in retinal lysates from exosome-inhibited mice, and controls. The expression of these genes and miRNA was measured using mouse specific TaqMan hydrolysis probes (**Table 1**) and TaqMan Gene Expression Master Mix (Thermo Fisher Scientific, MA, United States). Reactions were performed in technical duplicates in a 384-well format using a QuantStudio 12 K Flex RT-PCR machine (Thermo Fisher Scientific, MA, United States). Data was analyzed using the comparative C_t method ($\Delta\Delta C_t$) and results are presented as percent change relative to control. Expression was normalized to reference gene glyceraldehyde-3-phosphate dehydrogenase (*Gapdh*) for mRNA, and small nuclear RNA U6 for miRNA.

TABLE 1 | TaqMan hydrolysis probes (Thermo Fisher Scientific, MA, United States) used for qPCR.

Gene symbols	Gene name	Catalog number
miR-124a	Mmu_miR-124-3p	001182 (assay ID)
U6 snRNA	Small nuclear RNA U6	001973 (assay ID)
Gapdh	Glyceraldehyde-3-phosphatase dehydrogenase	Mm01536933_m1
Pdcd6ip	Programmed cell death 6 interacting domain	Mm00478032_m1
Smpd3	Sphingomyelin phosphodiesterase 3	Mm00491359_m1

Small RNA High-Throughput Sequencing

Library Preparation and Sequencing

cDNA libraries from miRNA-enriched s-mEV RNA samples were prepared by the John Curtin School of Medical Research Biomolecular Research Facility (JCSMR, BRF, ACT, Australia), using the Capture and Amplification by Tailing and Switching method (CATS RNA-seq Kit v2 × 24, Diagenode Cat# C05010041, Leige, Belgium). 10 ng RNA was used as input and the dephosphorylation step omitted to select for 3′-OH RNA species (miRNA). The library was amplified with 9 PCR cycles and cleaned with 0.9x AMPure® XP beads (A63881, Beckman Coulter, CA, United States) to enrich for DNA fragments shorter than 50 nt. Libraries were multiplexed and sequenced on a single lane using the Illumina NextSeq500 (Illumina, CA, United States) acquiring 50 base-pairs single-end reads. The sequencing depth was between 8 and 15 million reads/sample with an average phred read quality of 33 (**Supplementary Figure S3A**). Sequencing libraries prepared from whole retinal tissue were retrieved from BioProject database (Accession ID: PRJNA606092)[1]. These libraries were previously prepared by our group using the same library construction method, and the same bioinformatic analysis pipeline was applied as stated below, see Section "Bioinformatics."

Bioinformatics

Sequencing reads were initially checked for quality scores, adapter/index content and K-mer content using FastQC v0.11.8 (Babraham Bioinformatics, Cambridge, United Kingdom), then imported into Partek® Flow® (Partek Inc, MO, United States) for all subsequent analyses. Base composition analysis indicated the presence of an enriched poly-A tail and the CATS template-switching nucleotide within the first three base-pairs of the reads (**Supplementary Figure S3B**), indicating a successful library preparation. A trimming pipeline was created according to the following cutadapt code "cutadapt –trim-n -a GATCGGAAGAGCACACGTCTG -a AGAGCACACGTCTG < input.file > | cutadapt -u 3 -a AAAAAAAAAACAAAAAAAAAA -e 0.16666666666666666 - | cutadapt -g GTTCAGAGTTCTACAGTCCGACGATC -m 18 -o < output.file > -", to remove the template switching nucleotide and the 3′ and 5′ adapters associated with the CATS library preparation. After trimming, the base composition was centered around 25% for each nucleotide (**Supplementary Figure S3C**), and FastQC analysis confirmed the effective removal of the 3′ and 5′ adapters and indices.

Trimmed reads were aligned against the mature mouse miRNA downloaded from miRbase v.22 using the Burrows–Wheeler Aligner (BWA) in backtrack mode with parameters -n 1(base), -o 1, -e -1, -d 10, -i 5, -k 2, -E 4, -R 30, -t 24 (as recommended by Ziemann et al., 2016). miRNAs with less than 10 alignments across all samples were discarded from the subsequent analyses. Reads aligned to miRbase v.22 (mature

[1]https://www.ncbi.nlm.nih.gov/bioproject/?term=PRJNA606092

miRNAs) with BWA had a length distribution between 18 and 24 nucleotides consistent with the expected length of mature miRNA (**Supplementary Figure S3D**). Aligned reads were normalized using the Trimmed means of M (TMM) and Upper Quartile (UQ) methods as recommended (Tam et al., 2015), with the latter being chosen as the preferred method as it produced less variable means and distributions (**Supplementary Figures S3E–G**). After normalization, a two-dimensional principal component analysis (PCA) was performed in Partek® Flow® (Partek Inc, MO, United States) to assess the clustering of the samples and identify outliers. Fold changes and statistical significance were computed using the Gene Specific Analysis (GSA) tool within Partek® Flow® (Partek Inc, MO, United States). This function uses the corrected Akaike Information Criterion to select the best statistical model for each gene from the available Normal, Negative Binomial, Lognormal or Lognormal with shrinkage options. Lognormal with shrinkage (Wu et al., 2013), produced the best fit and thus was selected to perform differential analysis. A dataset was created containing the expression values for each miRNA in all samples and imported into R (R Core Team, 2019). The counts were $\log_2$ transformed to display the distribution of miRNAs in dim-reared and photo-oxidative samples using the packages ggbeeswarm (Erik, 2017) and ggplot2 (Wickham, 2016). Hierarchical clustering analysis (HCA) was performed in Partek® Flow® (Partek Inc, MO, United States) using the Euclidian distance as a point metric distance and the average linkage as the agglomerative method.

Sequencing data can be accessed from BioProject (Accession ID: PRJNA615966)[2].

Network and Pathway Enrichment Analysis

The miRNet platform (Fan et al., 2016) was used to elucidate potential interactions between s-mEV miRNA and retinal mRNA. The mRNA dataset is available from BioProject (Accession ID: PRJNA606092) (see text footnote 1) and comprises of all retinal genes with a $\log_2$(count per million) value > -2.4 (**Supplementary Table S2**). The retinal targetome of the top 10 s-mEV miRNAs as well as the targetome of the s-mEVs enriched miRNA were separately imported into Enrichr (Chen et al., 2013) and analyzed for over-expressed pathways annotated in Wikipathways (Slenter et al., 2018) (mouse annotation), and gene-disease associations listed in DisGeNet database (Piñero et al., 2016).

In vitro Experiments

661W Cell Culture

Murine photoreceptor-derived 661W cells (kindly gifted by Dr. Muayyad R. Al-Ubaidi, Department of Biomedical Engineering, University of Houston, Houston, TX, United States) (Al-Ubaidi et al., 1992), were used for *in vitro* experiments at passage 1–5. The authenticity of the of the cells was validated by short tandem repeat analysis (CellBank, Sydney, Australia). Cells were cultured in growth media [Dulbecco's Modified Eagle Medium (DMEM; Sigma-Aldrich, MO, United States) supplemented with 10% fetal bovine serum (FBS; Sigma-Aldrich, MO, United States), 6 mM L-glutamine (Thermo Fisher Scientific, MA, United States) and antibiotic-antimycotic (100 U/ml penicillin, 100 μg/ml streptomycin; Thermo Fisher Scientific, MA, United States)], as previously published (Lu et al., 2018). Cells were maintained and all incubation steps were performed in dark conditions in a humidified atmosphere of 5% CO_2 at 37°C, unless otherwise stated. Cells were passaged by trypsinization every 3 – 4 days.

To deplete FBS of s-mEV, the serum was centrifuged (200,000 × *g*, at 4°C for 18 h) using a Beckman Coulter Optima XE-100 Ultracentrifuge (Beckman Coulter, CA, United States), with a SW41Ti rotor (Beckman Coulter, CA United States) and the supernatant used as FBS supplement in all GW4869 experiments (adjusted growth media).

In vitro Photo-Oxidative Damage

661W cells were seeded in 96 well plates (Nunc, Thermo Fisher Scientific, MA, United States) at 2×10^4 cells/well 24 h prior to photo-oxidative damage experiments. Cells were exposed for 4 h to 15,000 lux light (2.2 mW/cm^2; irradiance measured with PM100D optical power meter, Thorlabs, NJ, United States) from two white fluorescent lamps (2 × 10W T4 tri-phosphor 6500K daylight fluorescent tubes; Crompton, NSW, Australia) as published previously (Lu et al., 2017; Fernando et al., 2018). Control cells were completely wrapped in aluminum foil with six small incisions to allow air/gas exchange.

Cell Viability by MTT Assay

Cell viability was tested by 3-(4,5-dimethylthiazol-2-yl)-2,5-diphenyltetrazolium bromide (MTT) assay (Roche, Mannheim, Germany), according to manufacturer's instructions. Briefly, conditioned media from 661W cells undergoing photo-oxidative damage or grown under dim conditions and treated with GW4869 at 5, 10, 20, and 40 μM concentrations or equivalent concentrations of DMSO was discarded and 100 μl growth media containing 10% MTT was added to all wells. The cells were incubated for 4 h to allow for the formation of formazan crystals then 100 μl of solubilization buffer was added to each well and cells incubated for 18 h. The absorbance at 570 nm of each well was measured with a 670 nm reference wavelength using an Infinite® 200 Pro plate reader (Tecan, Mannedorf, Switzerland). Background absorbance (wells containing medium with MTT reagent only) was subtracted from all sample wells and the viability calculated by dividing the absorbance of treated wells (DMSO or GW4869) by controls (cell treated with medium only).

Exosome Inhibition in 661W Cells

To test the effect of GW4869 on exosome inhibition, 661W cells were seeded at a density of 1×10^5 cells/well in 6 well plates (Nunc, Thermo Fisher Scientific, MA, United States) and grown to 80% confluence in growth medium. Media was removed and cells treated with 20 μM GW4869, or equivalent DMSO, in adjusted growth media for 4 h. The conditioned medium from four GW4869-treated or control wells (661W cells treated with equivalent DMSO concentration) was pooled and processed for s-mEV isolation and characterization as described in Sections "Retinal s-mEV isolation" and "NanoSight."

[2]https://www.ncbi.nlm.nih.gov/bioproject/?term=PRJNA615966

Statistical Analyses

All graphing and statistical analyses were performed using Prism V7.0, unless otherwise specified. An unpaired Student's *t*-test, one-way analysis of variance (ANOVA), or two-way ANOVA with Tukey's multiple comparison *post hoc* test was utilized as appropriate to determine the statistical outcome. Non-adjusted *p*-values ($P < 0.05$) or false-discovery adjusted *p*-values (FDR < 0.1) were deemed statistically significant. All data was expressed as the mean ± SEM.

RESULTS

Retinal s-mEV Isolation

In this work we demonstrate a novel protocol for the isolation of s-mEV from mouse retinas (**Figure 1A**). EVs isolated from dim-reared retinas displayed properties of s-mEV, including the distinctive round, cup-shaped morphology of exosomes (Jung and Mun, 2018) as seen in representative negative-stained TEM images (**Figure 1B** and **Supplementary Figure S1A**). Isolated vesicles were within the expected size-range of s-mEV including exosomes (Théry et al., 2002; Hessvik and Llorente, 2018; Słomka et al., 2018; Théry et al., 2018), as shown by TEM size distribution histogram, nanotracking analysis using NanoSight NS300 and dynamic light scatter using a Zetasizer Nano instrument (**Figures 1C–F**). Further, isolated vesicles displayed known s-mEV markers CD63, CD81, and CD9, as determined by western blotting (**Figure 1G**).

Retinal s-mEV Decrease in Concentration but Not Size, During Photo-Oxidative Damage-Induced Degeneration

Following the characterization of retinal s-mEV isolated from dim-reared retinas, the effect of photo-oxidative damage on the secretion of s-mEV was investigated (**Figure 2A**). The relative retinal s-mEV concentration was found to decrease in a damage-dependent manner, reducing significantly from dim-reared controls by 17 ± 2.7% after up to 3 days of photo-oxidative damage and 38 ± 4.0% after 5 days of photo-oxidative damage (**Figure 2B**). S-mEV concentration after 5 days of photo-oxidative damage was decreased from $(4.27 \pm 0.2) \times 10^{10}$ vesicles/ml to $(2.82 \pm -0.3) \times 10^{10}$ vesicles/ml (**Figure 2C**). The analysis of the size distribution of s-mEV at these two timepoints showed that vesicles with diameter of up to 200 nm had a more pronounced decrease in numbers (**Figure 2D**). The mean and modal size of s-mEV remained unchanged after 5 days of photo-oxidative damage (**Figure 2E**). Taken together these results suggest that while there is no change in the size of isolated s-mEV, there was a progressive reduction in the concentration of exosomes during photo-oxidative damage-induced degeneration.

GW4869 Inhibits s-mEV Bioavailability *in vitro*

Given the correlation between increased photoreceptor cell death and reduced retinal s-mEV concentration during photo-oxidative damage, the effect of s-mEV, specifically exosome inhibition was investigated using GW4869. To determine efficiency, GW4869 was added in culture to 661W photoreceptor-like cells (**Figure 3A**). s-mEV isolated from 661W were characterized using TEM (**Figure 3B** and **Supplementary Figure S1B**). Compared to DMSO controls, 661W s-mEV concentration (**Figures 3C,D**) was significantly reduced in GW4869-treated cells, demonstrating a high level of efficacy of this inhibitor. Furthermore, increased GW4869 concentrations did not affect cell viability compared to DMSO controls under dim conditions. However, following photo-oxidative damage (4 h of 15,000k lux white light), an inverse dose-dependent correlation was observed between GW4869 concentration and cell viability (**Figures 3E,F**). Overall GW4869 was shown to reduce the bioavailability of isolated s-mEV *in vitro,* with the reduction likely attributed to a decrease in exosome production.

Endocytic Pathway Inhibition Results in Reduced s-mEV Bioavailability *in vivo*

The contribution of exosomes to retinal s-mEV population was investigated *in vivo* (**Figures 4A,B**). s-mEV isolates from retinas of GW4869-treated mice (daily IP injections for 5 days) were reduced in concentration compared to those from DMSO-injected controls. This was seen in both dim-reared and photo-oxidative damaged retinas (**Figures 4C,D**). Additionally, the expression of genes associated with ESCRT-dependent and ESCRT-independent exosome biogenesis pathways were measured by qRT-PCR. We targeted *Pdcd6ip* (also known as *Alix*), which encodes an accessory protein in the ESCRT-dependent pathway, and *Smpd3*, which encodes nSMase2 in the ESCRT-independent pathway (Hessvik and Llorente, 2018). Retinal lysates from dim-reared and 5-day photo-oxidative damaged retinas as well as lysates from GW4869 and DMSO-injected photo-oxidative damaged retinas were used. The expression of *Pdcd6ip* and *Smpd3* was significantly increased in 5-day photo-oxidative damaged retinas compared to dim-reared controls (**Figure 4E**). Conversely, *Pdcd6ip* and *Smpd3* were found to be significantly reduced in GW486-injected retinas compared to DMSO-injected controls (**Figure 4F**). These results demonstrate that GW4869 can be used as an inhibitor of exosome production, and that exosomes likely contribute to the population as well as effects of retinal s-mEV.

Exosome Inhibition Reduces Retinal Function in Dim-Reared Mice

The effect of GW4869-mediated exosome inhibition on retinal health was investigated in dim-reared mice (**Figure 5A**). Retinal function was assessed using electroretinography (ERG). We show that GW4869-treated mice had reduced retinal function for both a-wave and b-wave measures (**Figures 5B–D**), compared to DMSO injected controls. To investigate this further, we measured photoreceptor cell death by counting $TUNEL^+$ cells in the outer nuclear layer (ONL). The inflammatory response was also measured by counting $IBA\text{-}1^+$ cells in the outer retina. No significant difference in either measure was observed between GW4869-injected and DMSO treated retinas

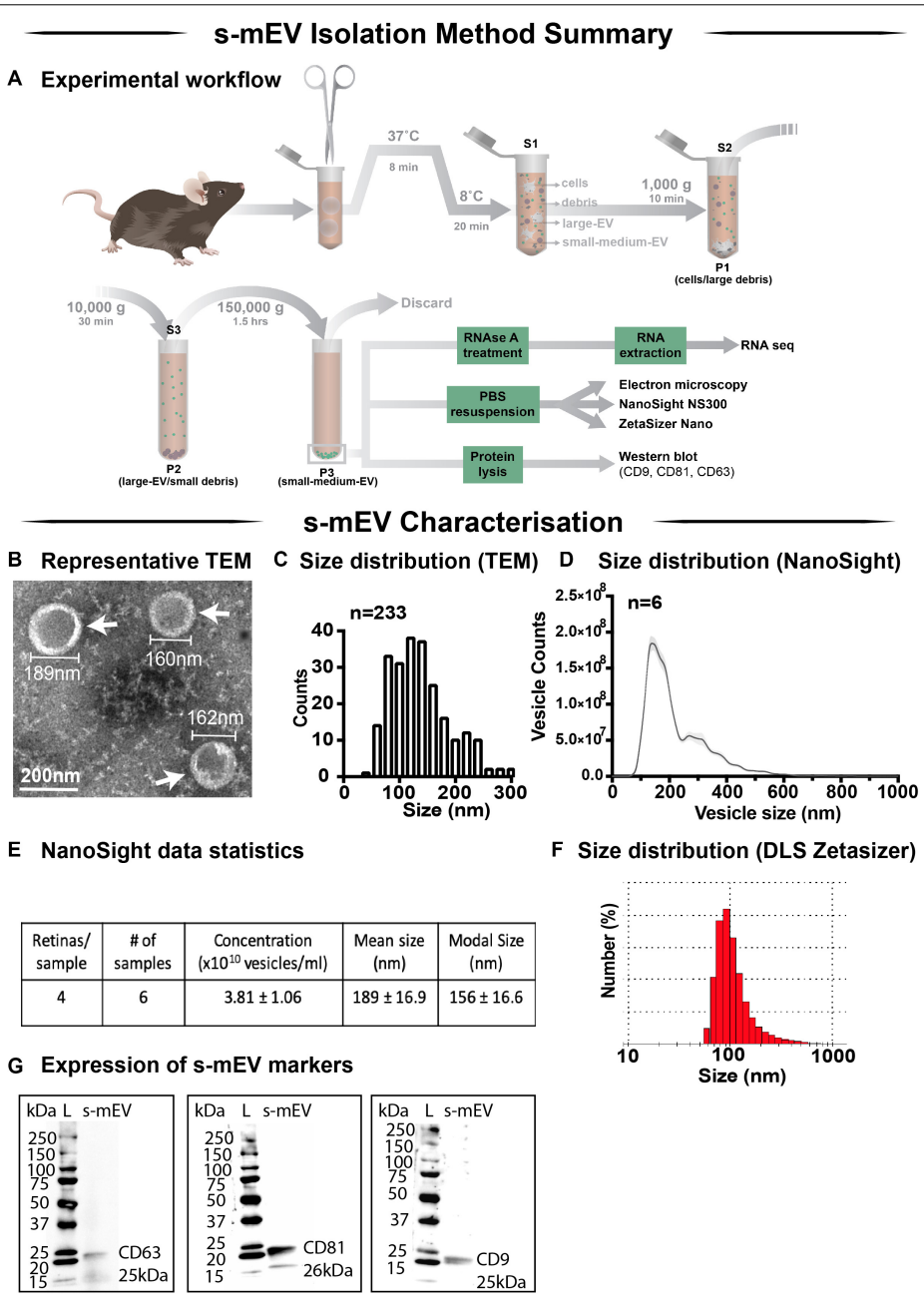

Retinas/ sample	# of samples	Concentration (x10^{10} vesicles/ml)	Mean size (nm)	Modal Size (nm)
4	6	3.81 ± 1.06	189 ± 16.9	156 ± 16.6

FIGURE 1 | Retinal s-mEV isolation and characterization. **(A)** Workflow for the isolation and characterization of retinal s-mEV. s-mEV were isolated from papain-digested retinas using differential ultracentrifugation. s-mEV pellets (P3) were processed for RNA extraction and RNA sequencing (RNA seq) and size and morphology analysis by electron microscopy, NanoSight NS300 and Zetasizer Nano. s-mEV pellets were also digested in protein lysis buffer and analyzed for the expression of s-mEV markers CD9, CD81, and CD63 by western blot. S, supernatant; P, pellet. **(B)** Representative Transmission Electron Microscopy (TEM) micrograph showing isolated retinal vesicles (white arrows) with consistent round, cup-shaped morphology and size of s-mEV. **(C)** Diameter distribution of retinal s-mEV measured from TEM micrographs (n = 233). **(D)** Size distribution of retinal s-mEV (n = 6 samples, 4 retinas/sample) using nanotracking analysis performed on a NanoSight NS300. **(E)** Average concentration, mean and modal size of s-mEV isolated from mouse retinas measured by nanotracking analysis (n = 6 samples, 4 retinas/sample). **(F)** Representative plot of the size distribution of s-mEV measured by dynamic light scatter (DLS) using a Zetasizer Nano instrument (n = 5). **(G)** Full-length western blots showing the presence of s-mEV markers CD63 (25 kDa), CD9 (26 kDa), and CD81 (25 kDa) in retinal s-mEV protein lysates. Molecular weight standard (L). Scale bar = 200 nm.

(**Figures 5E–G**). Additionally, photoreceptor cell death was also assessed by measuring the ratio of ONL thickness to total retinal thickness from OCT images. No significant difference was detected between the two groups (**Figures 5H,I**). Overall, while GW4869 impaired retinal function in dim-reared mice, no difference was observed in histological measures between

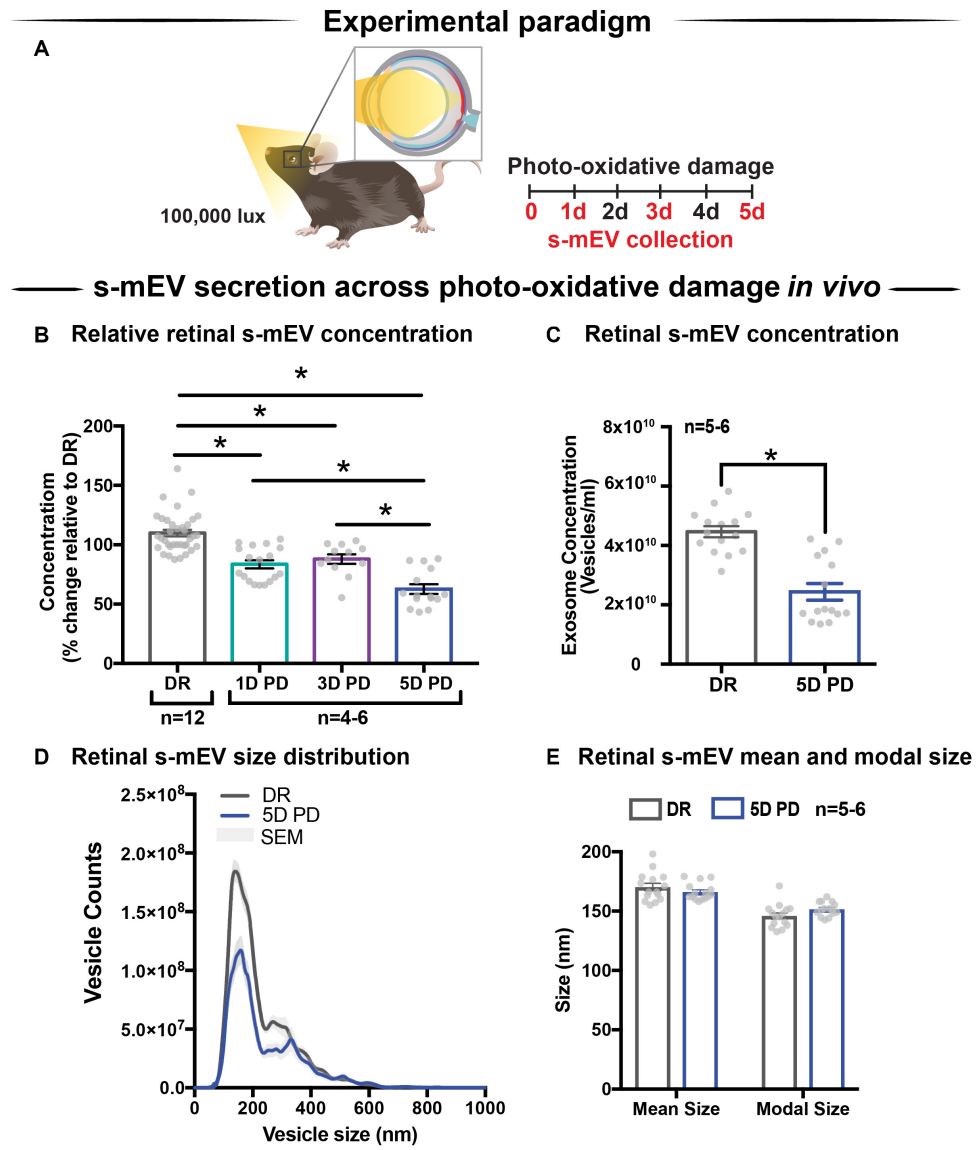

FIGURE 2 | Retinal s-mEV decrease in concentration but not size, over photo-oxidative damage-induced degeneration. **(A)** Experimental paradigm, with red retinal labeling indicating lesion site. **(B)** Concentration of retinal s-mEV decreased progressively across time in PD, with significantly reduced s-mEV at 1D, 3D, and 5D PD compared to DR controls ($P < 0.05$, $n = 3$–12). Concentration values are presented as percentage of DR. **(C)** Significant reduction in the concentration of s-mEV from 5D PD retinas compared to DR controls ($P < 0.05$, $n = 5$–6). **(D)** No significant change in the size distribution of s-mEV isolated from 5D PD retinas compared to DR controls, however vesicles with size <200 nm show a marked decrease in concentration following 5D PD ($P > 0.05$, $n = 5$–6). **(E)** No difference in either the mean or modal size of retinal s-mEV between DR and 5D PD groups ($P > 0.05$, $n = 5$–6). All results obtained using nanotracking analysis (NanoSight NS300). * denotes = $P < 0.05$.

GW4869-injected mice and DMSO controls over the 5-day period investigated.

Exosome Inhibition Reduces Retinal Function and Increases Cell Death and Immune Cell Recruitment in 5-Day Photo-Oxidative Damaged Mice

Given the reduction in ERG responses in GW4869-treated dim-reared mice, the effect of exosome inhibition was further investigated in mice subjected to 5 days of photo-oxidative damage (**Figure 6A**). GW4869-injected 5-day photo-oxidative damaged mice showed significantly reduced retinal function for both a-wave and b-wave measures (**Figures 6B–D**), compared to DMSO controls. Interestingly, and contrasting to GW4869-treated dim-reared mice, we observed significantly higher levels of photoreceptor cell death ($TUNEL^+$) and immune cell recruitment ($IBA\text{-}1^+$) in GW4869-injected 5-day photo-oxidative damaged mice compared to DMSO controls (**Figure 6E**). The increased number of $IBA\text{-}1^+$ cells in the

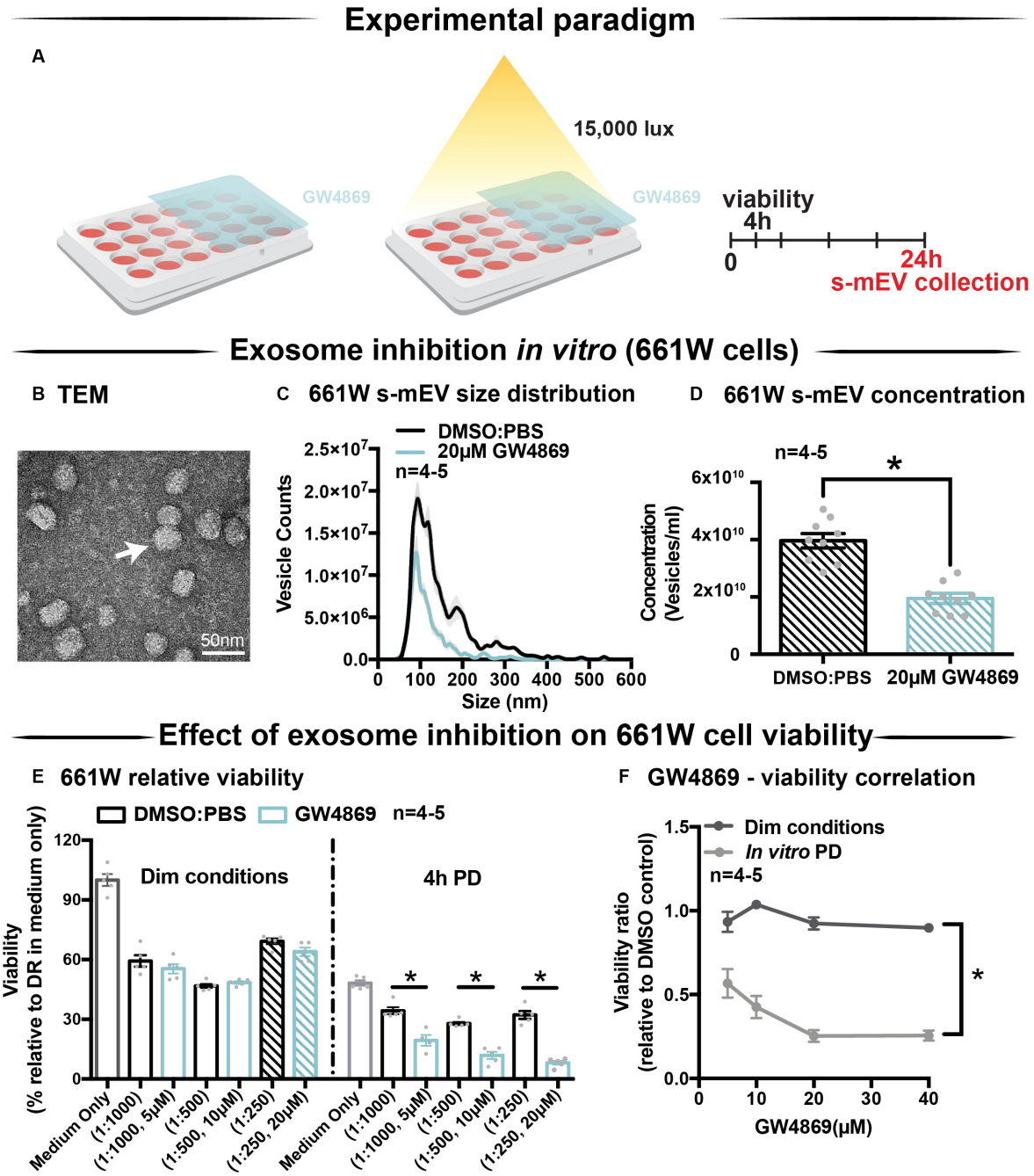

FIGURE 3 | GW4869 inhibits bioavailability of s-mEV *in vitro*. **(A)** Experimental paradigm. **(B)** Representative TEM micrograph showing isolated 661W vesicles. **(C,D)** s-mEV isolated from 661W photoreceptor-like cells in the presence of exosome inhibitor GW4869 (20 μM) or DMSO control for 24 h showed a significant reduction in concentration, as measured by NanoSight NS300. ($P < 0.05$, $n = 4–5$). **(E)** MTT assay to determine viability of 661W cells treated with increasing concentrations of GW4869 or DMSO. Results demonstrated no dose response in viability levels for either treatment under dim conditions, however, significant dose-dependent reduction in cell viability when treated with GW4869 under PD conditions ($P < 0.05$). **(F)** The viability ratio ($viability_{GW4869}/viability_{DMSO}$) of 661W cells treated with increasing concentrations of GW4869 in dim conditions or under 4 h PD showed no change while in dim conditions, however, is reduced between doses of 0–20 μM GW4869 before reaching a plateau by 40 μM while in PD conditions. Scale bar = 50 nm. *Patterned bars in **(E)** represent equivalent dosages/concentrations and conditions of GW4869/DMSO used in **(D)**. * denotes = $P < 0.05$.

outer retina included a higher ratio of amoeboid to ramified microglia and an increased presence of subretinal macrophages (**Figure 6E**). Further, there was a significant thinning of the ONL, indicating higher levels of photoreceptor cell death in GW4869-treated mice (**Figure 6F**). However, no difference in the thickness of the INL or GCL was observed (**Figure 6F**). Increased

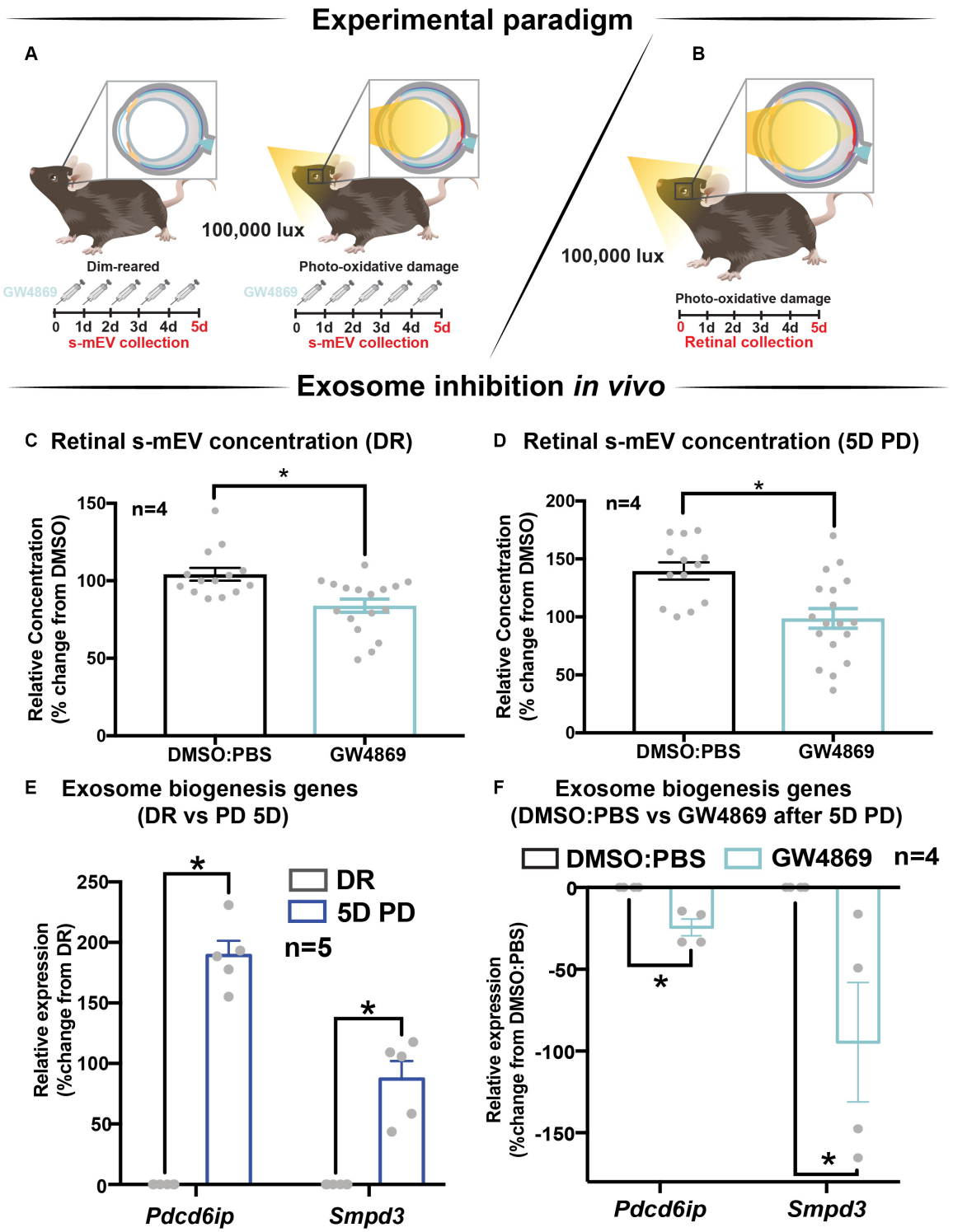

FIGURE 4 | GW4869 inhibits bioavailability of retinal s-mEV. **(A,B)** Experimental paradigm with red retinal labeling indicating lesion site. **(C,D)** Nanotracking analysis (NanoSight NS300) quantification revealed a significant reduction in the concentration of s-mEV isolated from both DR and 5D PD retinas following 5 daily intraperitoneal injections of GW4869 compared to respective DMSO controls ($P < 0.05$, $n = 4$). The expression of exosome biogenesis genes *Pdcd6ip* and *Smpd3* as measured by qRT-PCR was **(E)** significantly increased following 5D PD relative to DR controls ($P < 0.05$, $n = 5$) and **(F)** significantly reduced following daily injections of GW4869 while undergoing 5D PD, relative to DMSO injected controls ($P < 0.05$, $n = 4$). * denotes = $P < 0.05$.

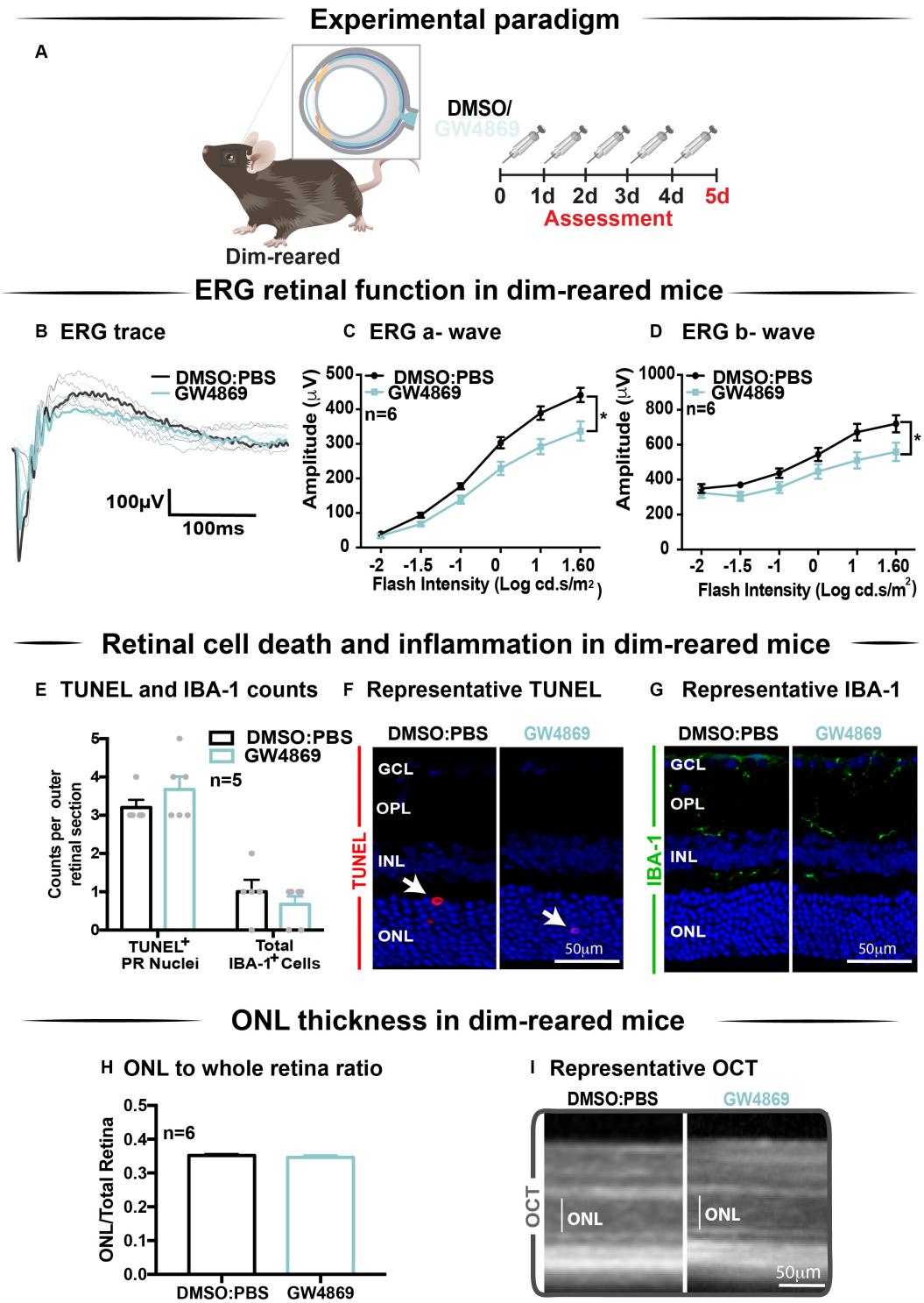

FIGURE 5 | Exosome inhibition via the use of GW4869 in dim-reared mice reduces retinal function. **(A)** Experimental paradigm. Following 5 daily intraperitoneal injections of GW4869 (1.25 mg/kg), retinal ERG function, **(B)** shown in representative ERG traces, was significantly reduced for both **(C)** a-wave and **(D)** b-wave responses, compared to DMSO controls in DR mice ($P < 0.05$, $n = 6$). **(E)** No significant changes were seen in either the number of TUNEL$^+$ cells in the outer nuclear layer, or in the number of IBA-1$^+$ cells in the outer retina following 5 daily intraperitoneal injections of GW4869 compared to DMSO controls ($P > 0.05$, $n = 5$). Representative confocal images show **(F)** TUNEL$^+$ cells (white arrows) and **(G)** IBA-1$^+$ cells in the outer retina, in both GW4869 and DMSO injected DR mice. Representative confocal images are taken in the superior outer retina, 1 mm from optic nerve head. **(H)** There was no change in ONL thickness (represented as ratio to total retinal thickness), as measured by ocular coherence tomography (OCT) between GW4869 or DMSO injected DR mice ($P > 0.05$, $n = 6$). **(I)** Representative images of OCT scans show ONL thickness in superior retina, (white line) in GW4869 and DMSO injected DR mice. Scale bars = 50 µM. * denotes = $P < 0.05$.

levels of photoreceptor cell death in GW4869-injected photo-oxidative damage mice were further demonstrated by a reduction of photoreceptor nuclei in the ONL (**Figure 6G**). Representative confocal images demonstrate an increase in photoreceptor cell death with significantly more TUNEL^{+} cells and thinner ONL (**Figure 6H**), as well as increased IBA-1^{+} cells (**Figure 6I**), in GW4869-treated mice compared to controls. Taken together these results show that exosome inhibition in retinas subjected to photo-oxidative damage causes reduced retinal function, concomitant with increased photoreceptor cell death and increased recruitment and activation of microglia/macrophages.

Retinal s-mEVs Possess a Distinct miRNA Profile Compared to the Retina Which Remains Unchanged Over 5-Days of Photo-Oxidative Damage

To obtain pure s-mEV-derived RNA, s-mEV isolated from dim-reared and 5 days photo-oxidative damaged retinas were treated with RNaseA prior to RNA isolation to remove potential contaminating RNA species attached to the outside. Bioanalyzer electropherograms show that RNaseA treatment successfully removed contaminating RNA, whereas s-mEV RNA was protected. Further, retinal s-mEV RNA was enriched for RNA species between 10 to 40 nucleotides (**Supplementary Figure S2**).

Databases of retinal and s-mEV miRNA were obtained using small RNAseq (**Figure 7A**), and were compared to determine if there was any selective enrichment of miRNA in isolated s-mEV. After generating normalized miRNA counts, a two-dimensional principal component analysis (PCA) was employed to visualize global differences between the expression of miRNA from dim-reared retinal s-mEVs and whole retinas. This analysis showed a clear segregation between the miRNA profiles of these groups (**Figure 7B**). Next, we examined the correlation between the expression levels of miRNAs from dim-reared retinal s-mEVs and whole retinas, finding a significant correlation (r = 0.71, $p < 0.0001$) between these groups. In particular, miR-183-5p, let-7b/c-5p, miR-124-3p, miR-125a/b-5p, and miR-204-5p were highly expressed in both groups (**Figure 7C**). This correlation analysis also indicated that some miRNA species were enriched in s-mEVs over the retina, with differential expression analysis uncovering that 28 miRNAs are over-represented in s-mEVs (FC $> +2$, FDR < 0.05), including miR-3770b, miR-706, miR-669c-3p, miR-7020-3p, and miR-3770 which were all over 100-fold more abundant (**Figure 7D**).

Following, we examined the differential expression in miRNA between dim-reared and photo-oxidative damaged-isolated s-mEVs. PCA showed no clustering of the samples suggesting that the miRNA contents of retinal s-mEV were not substantially altered following photo-oxidative damage (**Figure 7E**). Hierarchical clustering analysis (HCA) further illustrated this, with no significant clustering between dim-reared and 5 days photo-oxidative damage groups (**Figure 7F**). In line with the PCA and HCA, differential expression analysis revealed that only miR-1249-3p was differentially expressed (p-value = 0.046, fold change = −2.08) (**Figure 7G**). However, when adjusting for multiple comparisons (Benjamini–Hochberg), this miRNA did not pass the significance threshold (**Supplementary Table S1**).

A total of 154 miRNAs were detected in retinal s-mEV (**Supplementary Table S1**) showing a similar mean count distributions in both groups (**Figure 7H**). The top 10 most highly expressed miRNAs were consistent in both dim-reared and 5 days photo-oxidative damaged retinal s-mEV, and accounted for approximately 67% of the total miRNA counts (**Figure 7I**). miR-124-3p was the most abundant s-mEV-miRNA representing 17.5 and 16.3% in dim-reared and 5 days photo-oxidative damaged retinal s-mEV, respectively (**Figure 7I**). Four members of the let-7 family (let-7c-5p, let-7a-5p, let-7b-5p, and let-7f-5p) as well as miR-183-5p, miR-125a-5p, miR-125b-5p, miR-706, and miR-204-5p comprised the rest of the top 10 most highly abundant s-mEV-miRNA (**Figure 7I**). These results demonstrate the selective enrichment of miRNA in s-mEV from the retina, but that the miRnome of s-mEV does not change in response to photo-oxidative damage.

s-mEV miRnome Is Associated With Inflammatory, Cell Death and Motility Pathways

Considering that s-mEV miRNAs were not altered following 5 days of photo-oxidative damage and that the top 10 most abundant miRNAs accounted for 67% of the total s-mEV miRNAome, we focused on these top 10 s-mEV-miRNAs. A network analysis was performed to understand the interactions between the top 10 s-mEV-miRNAs and the retinal transcriptome (**Figure 8A** and **Supplementary Table S2**). This was also performed for the enriched s-mEV miRNA. Network analyses of the top 10 most abundant s-mEV miRNA revealed that eight miRNAs form a regulatory network containing 1326 targets (**Figure 8Bi**), of which, miR-124-3p, mir-706 and let-7b-5p, have 472, 235 and 353 predicted interactions with retinal transcripts, respectively (**Supplementary Table S3**). Similarly, the retinal targetome of the miRNA showing preferential enrichment in s-mEVs was explored with miRNet showing that miR-466i-3p, miR-446i-5p, miR-let-7b-5p, miR-1195, and miR-706 all had over 100 predicted targets in the retina (**Figure 8Bii** and **Supplementary Table S4**). The predicted targets of both sets of miRNA were separately used for enrichment analyses against WikiPathways (mouse pathway annotation) and DisGeNET (database containing gene-disease associations) on the Enrichr platform. A total of 50 pathways were significantly over-represented in WikiPathways (**Supplementary Tables S5, S6**). Notably, pathways pertaining to inflammatory processes including IL-1 to IL-6 signaling, Toll-like receptor signaling and chemokine signaling showed a significant enrichment. Pathways related to cell survival and motility were also significantly enriched (**Figures 8C,D**), with apoptosis significantly associated with miRNA targets from s-mEV-enriched miRNA (**Figure 8C**). Finally, DisGeNET database analysis revealed a significant association between s-mEV-miRNA targets and 6 retinal diseases (**Figure 8E** and **Supplementary Table S7**), with the majority associated with an

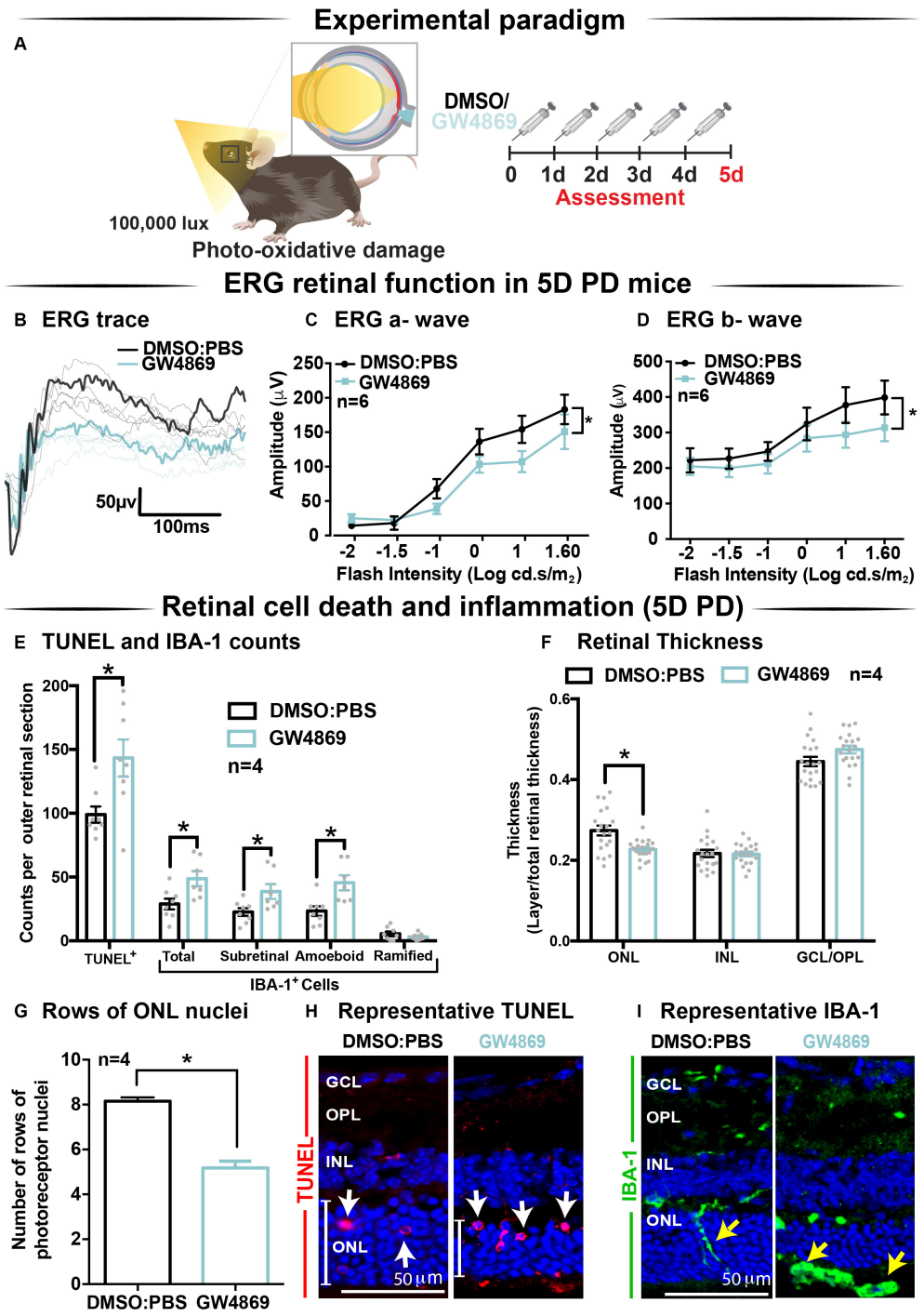

FIGURE 6 | Exosome inhibition via the use of GW4869 in mice subjected to 5 days photo-oxidative damage reduces retinal function and increases cell death and immune cell recruitment. **(A)** Experimental paradigm with red retinal labeling indicating lesion site. Following 5 daily intraperitoneal injections of GW4869 (1.25 mg/kg), retinal ERG function, **(B)** shown in representative ERG traces, was significantly reduced for both **(C)** a-wave and **(D)** b-wave responses, compared to DMSO controls in 5D PD mice ($P < 0.05$, $n = 6$). **(E)** There was a significant increase in the number of TUNEL$^+$ cells in the ONL, as well as a significant increase in the total number, number of subretinal, and number of amoeboid but not ramified IBA-1$^+$ cells in the outer retina in GW4869-injected mice compared to DMSO controls following 5D PD ($P < 0.05$, $n = 4$). **(F)** There was a significant reduction in the thickness of the ONL of GW4869-injected 5D PD mice compared to DMSO controls ($P < 0.05$, $n = 4$), however, no change was observed in the thickness of the INL or GCL between these groups ($P > 0.05$, $n = 4$). **(G)** The number of photoreceptor row nuclei in the ONL was also significantly reduced in GW4869-injected 5D PD mice compared to DMSO controls ($P < 0.05$, $n = 4$). Representative confocal images show **(H)** increased levels of TUNEL$^+$ cells (while arrow) and reduced ONL thickness (white line) as well as **(I)** increased number of IBA-1$^+$ cells in the outer retina, in GW4869-injected mice following 5 days of PD. Representative confocal images are taken in the superior outer retina, 1 mm from optic nerve head. Scale bars = 50 µM. * denotes = $P < 0.05$.

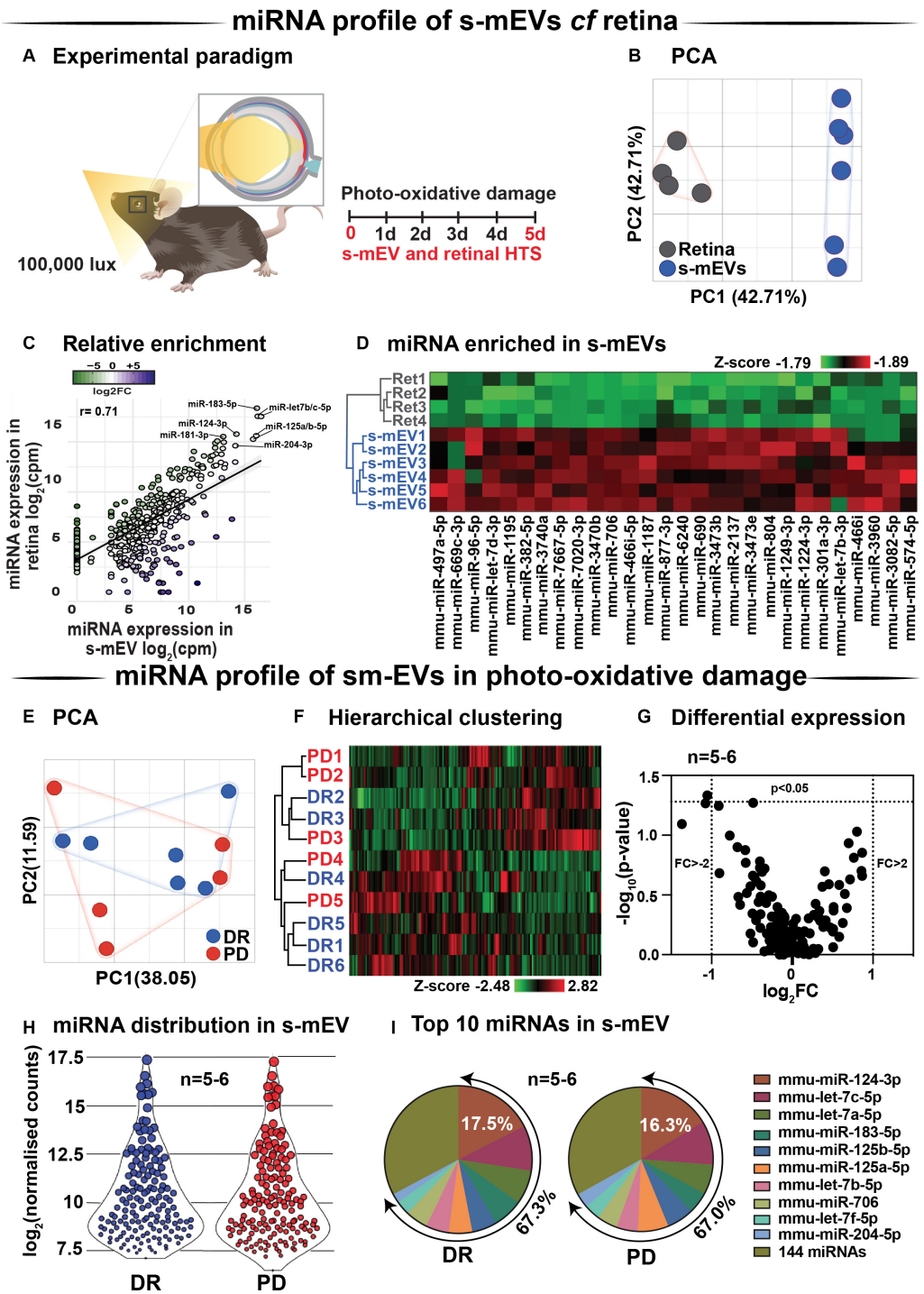

FIGURE 7 | s-mEV miRNA profiling and enrichment analysis. **(A)** Experimental paradigm with red retinal labeling indicating lesion site. **(B)** Principal component analysis (PCA) of retinal miRNA and s-mEVs miRNA showed clear clustering suggesting that each group possesses uniquely enriched miRNA. **(C)** A positive correlation was observed ($r = 0.71$, $p < 0.0001$) between miRNA counts in the dim-reared retina and s-mEVs with miR-124-3p, miR-181-3p, miR-204-3p, miR-125a/b-5p, and miR-let7a/b-5p being abundant in both. **(D)** Hierarchical clustering of miRNA showed significant enrichment of miRNA in s-mEVs compared to the dim-reared retina (FC > 2, FDR < 0.05). **(E)** PCA and **(F)** hierarchical clustering analysis show no grouping or miRNA between DR and PD samples and identified no outliers. **(G)** Volcano plot indicating that no differential analysis was observed in s-mEV from DR and 5D PD retinas ($P > 0.05$, $n = 5$-6). **(H)** Violin plots showing the distribution of miRNA transcripts in s-mEV from DR and 5D PD retinas ($n = 5$–6). Each data point represents the $\log_2$ transformed average number of counts for each miRNA retained after removing miRNAs with low expression and the size of each point is proportional to the average expression value of each miRNA. s-mEV from both DR and 5 days PD retinas contain similar amounts of miRNA transcripts with low, medium and high expression. **(I)** The top 10 most abundant miRNA were conserved in retinal s-mEV from DR and 5 days PD retinas and accounted for approximately 67% of the total counts.

inflammatory and/or proliferative profile. In summary, s-mEV miRNA cargo remains stable in the degenerating retina but the most abundant and enriched miRNA in s-mEV are predicted to modulate inflammation, cell death responses and cellular motility pathways.

s-mEV May Mediate the Translocation of miR-124-3p From the Outer to Inner Retina During Photo-Oxidative Damage-Induced Retinal Degeneration

We hypothesized that s-mEV may mediate the transportation of miRNA, including miR-124-3p, through the retina during damage. To test this, *in situ* hybridization of miR-124-3p was performed on retinal cryosections from mice injected daily with GW4869 and subjected to 5 days of photo-oxidative damage (**Figure 9A**). As previously reported (Chu-Tan et al., 2018), miR-124-3p expression was significantly increased in the INL after 5 days photo-oxidative damage compared to dim-reared controls (**Figures 9B,C**). Interestingly, GW4869 treatment significantly reduced photo-oxidative damaged-induced miR-124-3p expression in the ONL and INL but not ILM/IS (**Figures 9D,E**). This indicates that the within-retinal expression, and potentially movement of miR-124-3p in response to photo-oxidative damage may be mediated by s-mEV such as exosomes. To further explore our hypothesis, we examined the expression of miR-124-3p in photo-oxidative damaged retinas after treatment with GW4869 and observed no differential expression compared to DMSO-injected controls (**Figure 9F**). This indicates that the reduced expression of miR-124-3p in the ONL and INL is likely due to lack of transport into the INL rather than a decrease in total retinal expression. Given the increased levels of cell death and inflammation in mice treated with GW4869, we speculate that s-mEV shuttling of miRNA including miR-124-3p is required for normal retinal homeostasis and immune modulation.

DISCUSSION

This study describes for the first time, the isolation and characterization of mouse retinal s-mEV and the important role they play in retinal health and degeneration. We demonstrate four key findings from this study: Firstly, we demonstrate that s-mEV isolated from mouse retinas decrease in concentration progressively as a consequence of retinal degeneration. Secondly, we show that partial s-mEV depletion, via systemic administration of the exosome inhibitor GW4869, resulted in reduced retinal function in the normal retina and further exacerbated functional losses in mice subjected to photo-oxidative damage. Notably, significant photoreceptor cell death and inflammation were observed in GW4869-injected mice undergoing photo-oxidative damage, which was mirrored *in vitro* by 661W photoreceptor-like cells displaying increased susceptibility to photo-oxidative damage following exosome inhibition. Thirdly, we used small RNA sequencing and bioinformatic analyses to report on the potential regulatory roles of s-mEV miRNAs in retinal degeneration. Lastly, using the s-mEV-abundant miRNA miR-124-3p as a measure, we provide evidence that retinal s-mEV could be involved in the dynamic cell-to-cell transfer of miRNA in the degenerating retina. Taken together, we propose that retinal s-mEV and their miRNA cargo play an essential role in maintaining retinal homeostasis through immune-modulation, and that this effect is potentially mediated by s-mEV populations including exosomes.

Photoreceptor Cell Death Is Associated With Reduced s-mEV Bioavailability

Previous studies have demonstrated that miRNA-laden exosomes are found in abundance in the CNS and are central to cell-to-cell communication (Fauré et al., 2006; Lachenal et al., 2011). Although it is unclear which retinal cell type(s) s-mEV isolated in this work are secreted by, our evidence supports a photoreceptor-derived contribution. We demonstrate a progressive decrease in s-mEV numbers during photo-oxidative damage, which correlates with increasing levels of photoreceptor cell death as previously described in this model (Natoli et al., 2016). Therefore, we attribute the decrease in isolated retinal s-mEV to a loss of photoreceptors. In addition, the high abundance of photoreceptor prominent miRNAs miR-124-3p (Chu-Tan et al., 2018) and miR-183-5p (Xiang et al., 2017) in isolated retinal s-mEV, further attests to a potential photoreceptor origin, with miR-124-3p comprising 17.5 and 16.3% of the total s-mEV-miRnome in normal and damaged retinas, respectively.

Previous studies by Vidal-Gil et al. (2019) report that the exosome protein marker CD9 was localized to the photoreceptor inner segments and ONL, further supporting a photoreceptor-origin hypothesis. However, it should be noted that CD9 was also found in the INL, GCL and choroid. Using a genetic model (*rd10* mice) of retinitis pigmentosa, which results in progressive rod photoreceptor-specific cell death (Gargini et al., 2007; Vidal-Gil et al., 2019) showed that EVs isolated from retinal explants contain rhodopsin protein. This exosomal rhodopsin expression increased following photoreceptor rescue. Therefore, the authors describe EV secretion as a function of photoreceptor cell death, with significantly lower levels of CD9 expressing vesicles isolated from *rd10* mouse retinas at postnatal day 18 (P18) compared to at P16 (Vidal-Gil et al., 2019). Taken together these results demonstrate a clear relationship between retinal s-mEV secretion and photoreceptor cell survival, suggesting a significant s-mEV population may derive from photoreceptors in the retina.

Contrary to our findings, it is well established that a pro-oxidative stress or a proinflammatory environment often results in the increased release of exosomes (Lehmann et al., 2008; Essandoh et al., 2015; Benedikter et al., 2018; Hessvik and Llorente, 2018). We do observe increased expression of exosome biogenesis genes *Pdcd6ip* and *Smpd3* in retinal lysates following 5 days of photo-oxidative damage. We therefore suggest that all retinal cells including photoreceptors, as demonstrated by Vidal-Gil et al. (2019), may be potentially increasingly releasing s-mEV including exosomes as a consequence of the heightened presence of inflammatory and oxidative stress stimuli created in response to acute retinal degenerations. Further, we hypothesize

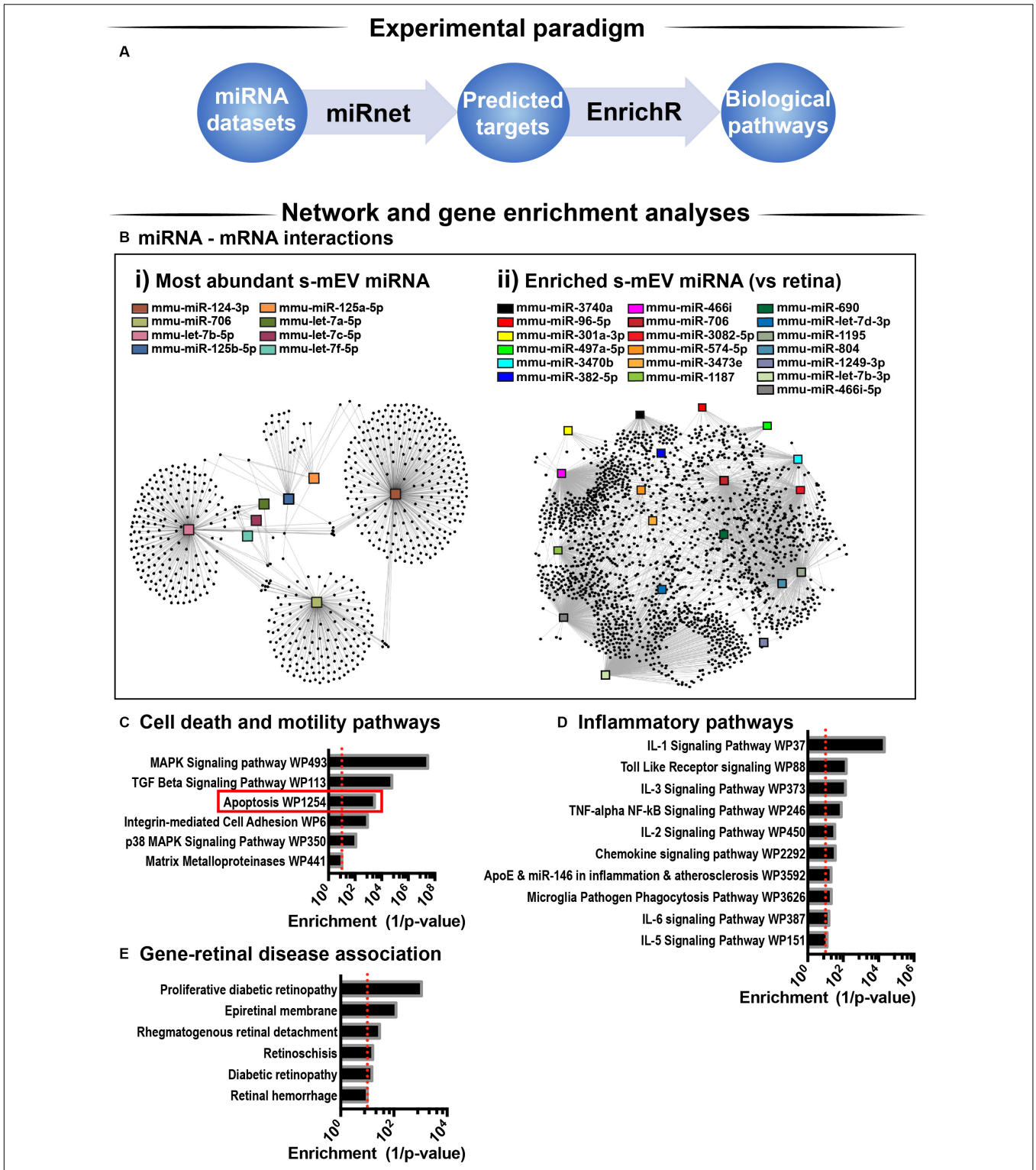

FIGURE 8 | s-mEV miRNA target and pathway analysis. **(A)** Analysis pipeline. **(B)** miRNet network analysis using the **(i)** top 10 most highly expressed s-mEV-miRNAs and **(ii)** miRNAs enriched in s-mEVs showed their predicted interactions with target mRNAs. From the top 10 most abundant s-mEV miRNAs, eight formed an interconnected network, with miR-124-3p, miR-706 and let-7b-5p having the largest number of predicted targets. From the most enriched s-mEVs miRNAs, miR-466i-3p, miR-466i-5p and miR-1195 had the largest targetomes. Pathway analysis was performed using the predicted targets of the most abundant **(Bi)** and most enriched **(Bii)** miRNA, collectively showing a significant enrichment of pathways pertaining to **(C)** cell survival and motility, **(D)** inflammatory processes and oxidative stress ($P < 0.05$). **(E)** Enrichment analysis was also performed against DisGeNet (database containing gene-disease associations) revealing that a number of retinal diseases were significantly associated with the targets of s-mEV-miRNAs ($P < 0.05$).

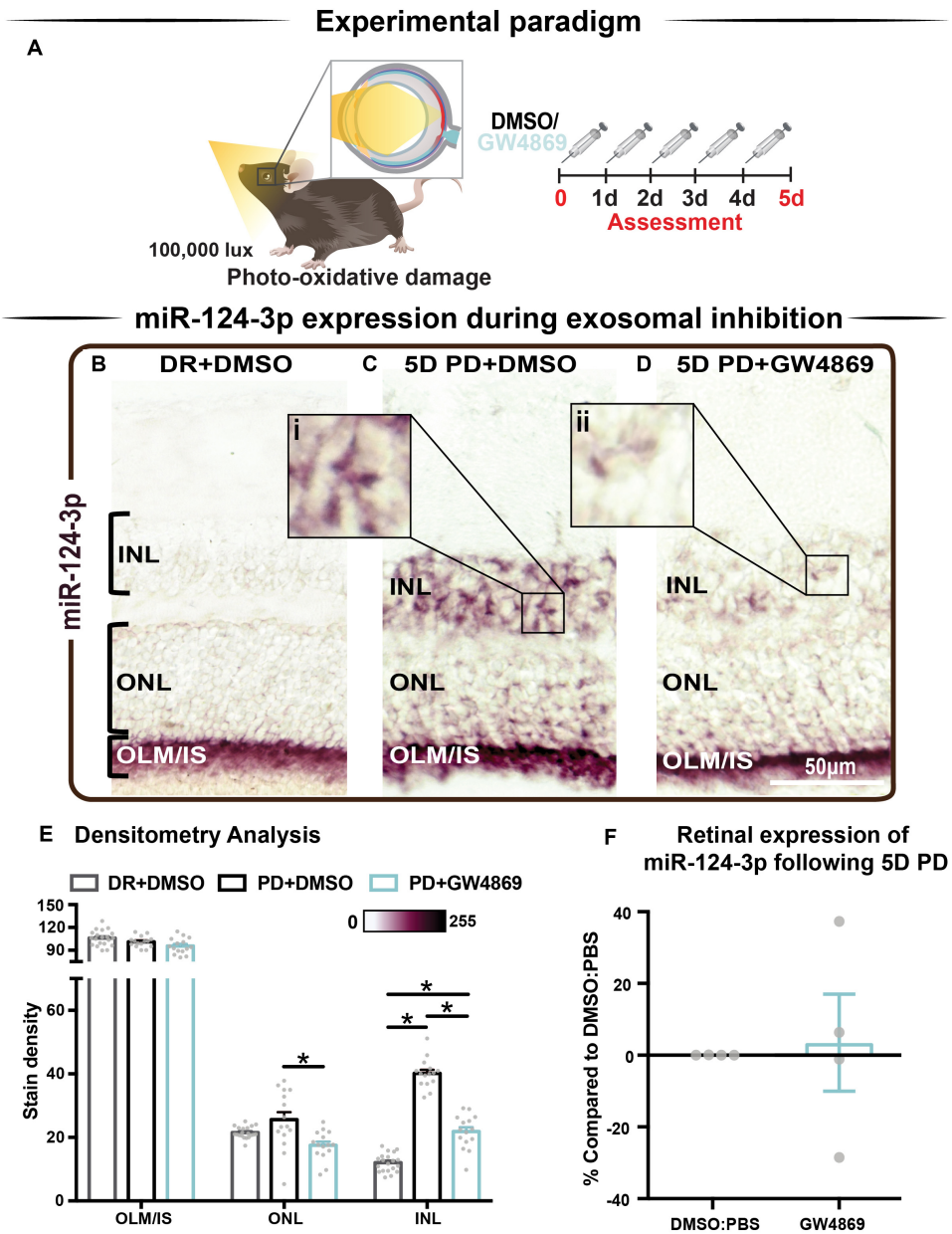

FIGURE 9 | s-mEV may mediate the translocation of miR-124-3p from the outer to inner retina during photo-oxidative damage-induced retinal degeneration. **(A)** Experimental paradigm with red retinal labeling indicating lesion site. **(B)** Using *in situ* hybridization, miR-124-3p expression in DR retinal cryosections was localized to the outer limiting membrane/photoreceptor inner segments (OLM, IS), however **(C)** following 5D PD, miR-124-3p was seen in the INL (inlet, **i**). **(D)** Following intraperitoneal administration of GW4869 exosome inhibitor, miR-124-3p expression is significantly reduced in the ONL and INL (inlet, **ii**). Representative images are taken in the superior outer retina, 1 mm from optic nerve head. **(E)** Densitometry analysis of miR-124-3p in retinal layers confirmed a decrease in miR-124-3p expression in the ONL and INL of mice treated with GW4869. **(F)** Retinal expression of miR-124-3p was conducted using qRT-PCR in photo-oxidative damaged mice treated with GW4869 or DMSO control, showing no change in total retinal expression ($P > 0.05$). Scale bar = 50 µM. * denotes = $P < 0.05$.

that photoreceptors, as the most abundant retinal cell type, are the largest contributor to the pool of retinal s-mEV and thus their loss leads to a net decrease in the total bioavailability of retinal s-mEV. Independent isolation and quantification of s-mEV and in particular exosomes from each major retinal cell type may shed some light in this regard and will be investigated in the future. We also note that it is also possible that the increased expression of *Smpd3* may be occurring as a result of degeneration, with nSMase2/ceramide-induced apoptosis reported in models of retinal degenerations (German et al., 2006; Chen et al., 2012; Simón et al., 2019). While we do not see a protection from cell death following treatment with GW4869, we suspect that reduced exosomal communication may supersede possible protective effects from nSMase2/ceramide inhibition. Investigations into the

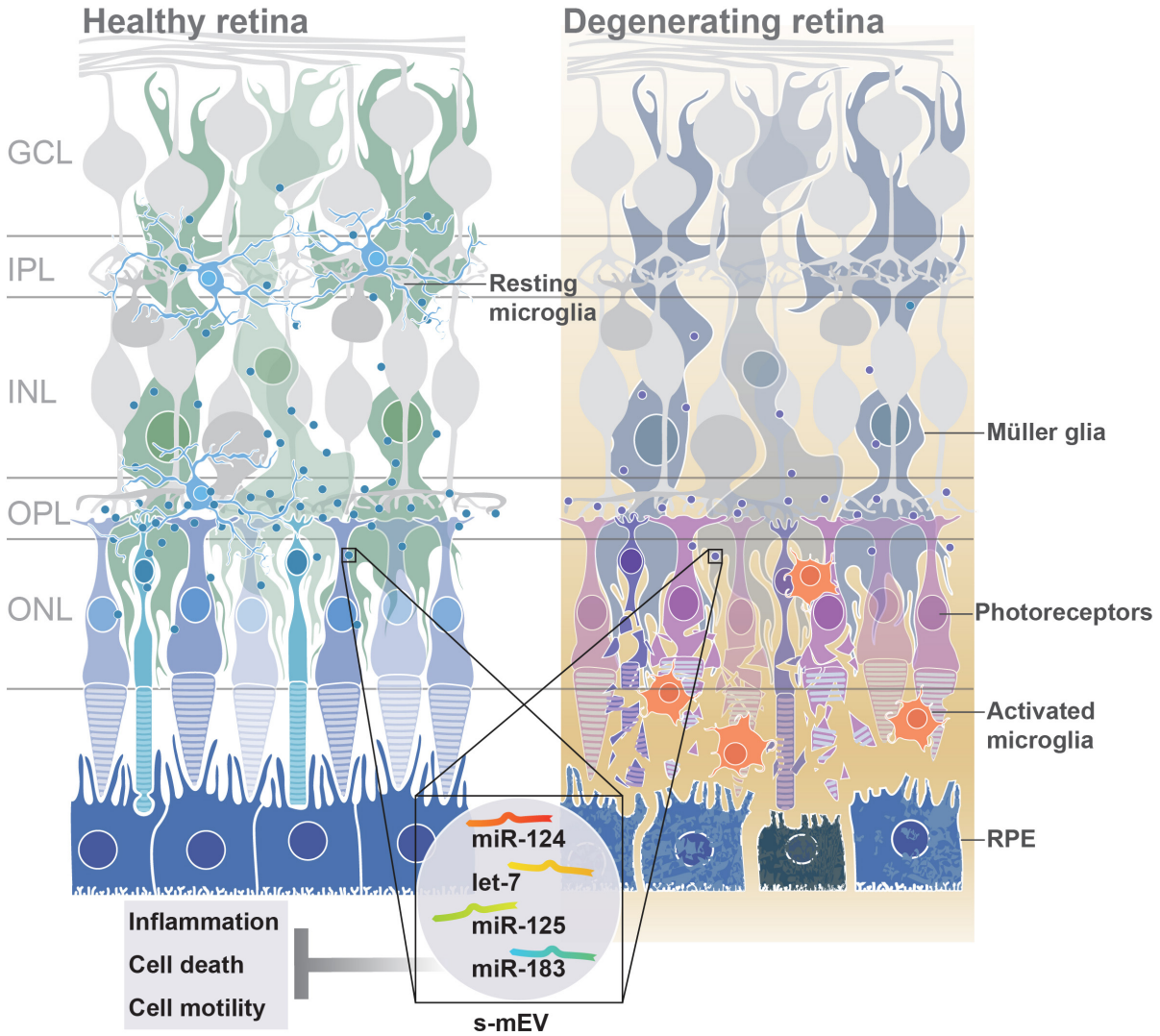

FIGURE 10 | Proposed functional role of s-mEV. Under normal homeostatic conditions, s-mEV laden with miRNA, including miR-124, let-7, miR-125, and miR-183, potentially originating from photoreceptors, are continuously trafficked between retinal neurons and glial cells. However, in retinal degenerations, a loss of photoreceptors leads to a decrease in s-mEV bioavailability, and consequently an insufficient transfer of s-mEV miRNA cargo to their cell targets. As the retinal targetome of s-mEV-miRNAs is associated with inflammation, survival and cell motility pathways, inadequate pathway regulation following s-mEV depletion leads to exacerbated retinal damage.

interplay between exosome release and retinal ceramide levels will be explored in future works.

An additional hypothesis is that in response to excessive light, increased numbers of retinal s-mEV are mobilized as early responders to stress. However, even by 1 day of photo-oxidative damage, have already been depleted past a homeostatic level, ensuing an inflammatory response. As we previously demonstrated the potential translocation of miR-124-3p to the INL within 24 h of damage (Chu-Tan et al., 2018), it seems possible that s-mEV transport of this miRNA could have occurred before this early time point as a rapid response to stress. In fact, Krol et al. (2010) demonstrated that photoreceptor-specific miRNAs such as miR-183/182/96 as well as miR-204 and miR-211 are modulated in response to light exposure as short as 3 h. We also identified mir-183/182/96, miR-204 and miR-211 in retinal s-mEV however, while Krol et al. (2010) do not propose a mechanism responsible for the miRNA turnover observed in their work, our work presented here suggests that s-mEV may be involved. Quantifying s-mEV secretion during early stress responses is required to determine if s-mEV depletion is a cause or consequence of retinal degeneration, and represents an important piece of the therapeutic puzzle.

Retinal s-mEV as Mediators of Immuno-Modulation

Regardless of origin, to date the role that s-mEV play in retinal health and disease is still largely unclear. Results from this

work strongly support a mechanism by which retinal s-mEV and in particular exosomes mediate homeostasis and immunomodulation, with the inhibition of exosomes using GW4869 both *in vitro*, and *in vivo*, resulting in increased cell death, as well as recruitment and activation of microglia/macrophages. Importantly these observations were only evident under stress conditions, with both control 661W cells and dim-reared retinas displaying no major signs of cell death or inflammation following exosome-inhibition in the absence of photo-oxidative damage. We suggest that unlike in the degenerating retina, that exosome inhibition had no major effects on cell health. This is likely to be a consequence of the experimental paradigm used in this study and the short period of inhibition, or alternatively could indicate that under stress exosomal communication is necessary for cell survival. A smaller average size was seen in 661W-isolated s-mEV compared to those from the retina, and while we attribute this to the heterogenous nature of whole tissue, it could suggest that photoreceptors primarily secrete a smaller s-mEV fraction such as exosomes, and it is this population that may mediate retinal damage. This hypothesis however requires further investigation.

We hypothesize that as a consequence of longer-term exosome inhibition, inadequate translocation of miRNA cargo via s-mEVs results in the dysregulation of immune pathways. We have previously reported that in response to photo-oxidative damage, miR-124-3p upregulation in the INL may occur via outer-to-inner retinal translocation, with miR-124-3p acting as an anti-inflammatory regulator of C-C Motif Chemokine Ligand 2 (Ccl2) to prevent the recruitment of microglia/macrophages (Chu-Tan et al., 2018). In this present study, we provide further evidence of s-mEV-mediated miRNA translocation, demonstrating that in mice treated with GW4869, INL upregulation of miR-124-3p, the most highly expressed miRNA in isolated retinal s-mEV, was reduced. Although correlative, we suggest that insufficient gene regulation due to reduced s-mEV/miRNA bioavailability could contribute to the increased presence of immune cells and inflammation as seen in retinal degenerations. While we do not exclude the possibility that miR-124-3p could be upregulated in the INL in response to photo-oxidative damage, and downregulated following treatment with GW4869, we believe that this is unlikely, given the lack of differential change in the expression of miR-124-3p in photo-oxidative damaged mice injected with GW4869 compared to controls. The s-mEV-dependent transport of miRNA in mediating immune regulation however requires further exploration particularly in regard to the hypothesized movement of s-mEVs in retinal damage. Future experiments should utilize EV reporter strains such as those generated by Men et al. (2019) as well as intra-ocular administration of fluorescently tagged s-mEVs to obtain direct evidence of s-mEV movement and uptake in the degenerating retina, and will be investigated in further detail in the future.

To further support the hypothesis that retinal s-mEV mediate homeostasis and immune responses, network and pathway analysis of retinal s-mEV-miRNAs revealed that the top 10 miRNA and miRNA enriched in s-mEVs were associated with the regulation of inflammatory and cell survival pathways. For example, our network analysis indicates that the top 10 miRNA are controlling genes associated with Interleukin and chemokine signaling, with both of these biological pathways involved in a plethora of retinal degenerative diseases (Rutar et al., 2015; Wooff et al., 2019). Moreover, MAPK signaling and TGF-β have also been shown to play pivotal roles in the development of retinal degenerations (Kyosseva, 2016; Wang et al., 2018), with both pathways showing a strong association with the targetome of the top 10 most highly expressed s-mEV-miRNAs. As the top 10 miRNAs in both dim-reared and photo-oxidative damage retinal s-mEV make up approximately 70% of the total s-mEV-MiRnome, it is not surprising that a reduction in s-mEV numbers during degeneration could lead to immune dysfunction due to inadequate gene regulation. In fact, as recently demonstrated by Bian et al. (2020) exosomes secreted from transplanted neural stem/progenitor cells (NPCs) in the subretinal space resulted in delayed photoreceptor cell death, preserved retinal function and the suppressed activation of retinal microglia. Further, this group demonstrated that the miRNA cargo of NPC exosomes mediated this protection, with many NPC-derived miRNA found to be similar to s-mEV-derived miRNA reported in this study (Bian et al., 2020). Enrichment analysis of retinal s-mEV-MiR revealed significant associations with retinal degenerative diseases such diabetic retinopathy, retinal detachment and retinal hemorrhage further highlighting their potential involvement in modulating retinal inflammatory diseases.

From these collective findings, we propose that in normal retinal health, s-mEV are secreted from photoreceptor cells, and are released to the surrounding retina to maintain a homeostatic environment. However, following photoreceptor cell death, we hypothesize that immune responses are no longer able to be regulated due to reduced s-mEV numbers and the bioavailability of miRNA cargo; leading to the upregulation of inflammatory pathways, infiltration and activation of microglia/macrophages and progressive retinal cell death (**Figure 10**); characteristic features of retinal degenerative diseases (Kauppinen et al., 2016; Rivera et al., 2017; Rübsam et al., 2018; Wooff et al., 2019).

s-mEV as Mediators of Phototransduction

In addition to a potential role as regulators of retinal homeostasis through immune modulation, we highlight a possible involvement of retinal s-mEV, and in particular exosomes, in phototransduction. In both dim-reared and photo-oxidative damaged mice, exosome inhibition resulted in reduced retinal function as measured by ERG. While we could attribute the loss of retinal function in photo-oxidative damage mice to increased levels of photoreceptor cell death and immune cell recruitment, dim-reared mice showed no detectable signs of either cell death or inflammation at the time-point investigated, yet still demonstrated significantly lower functional responses.

While the role of s-mEV and exosomes in phototransduction in the retina is currently unknown, in the CNS the

communication of exosomal cargo from oligodendrocytes and astrocytes has been reported to affect neurotransmission pathways (Antonucci et al., 2012; Fröhlich et al., 2014; Pascua-Maestro et al., 2018). In particular, Frühbeis et al. (2013) suggested that the exosome communication between oligodendrocytes and neuronal axons is triggered by glutamate release (Frühbeis et al., 2013). While oligodendrocytes are not present in the retina, Müller glia perform a similar role, responsible for the reuptake of glutamate released from photoreceptors terminals and the synaptic clefts of second order neurons as part of normal phototransduction (Bringmann et al., 2013). We speculate that, perturbations of exosomal communication systems could lead to aberrant glutamate reuptake by Muller cells and impaired signal transduction, explaining the observed reduction in retinal function of exosome-inhibited mice. However, this area requires further in-depth exploration.

The Role of Exosomes in Retinal Degenerative Diseases and Their Potential as Therapeutic Gene Therapy Vehicles

To date, little progress has been made in uncovering the role that s-mEV may play in the progression of retinal degenerations, and further how we can utilize s-mEV, their cargo, and/or biological targets in diagnostic panels and in therapeutic development. It has been recently shown in cell culture models (Kang et al., 2014; Atienzar−Aroca et al., 2016; Zhang et al., 2019), that following high levels of oxidative stress (pathologically relevant to the onset of many retinal degenerative diseases), increased exosome numbers containing high expression of vascular endothelial growth factor receptor (VEGFR) are secreted from a retinal pigmented epithelium (RPE) cell culture line (aRPE19) to promote neovascularization, a hallmark feature of several retinal pathologies (Atienzar−Aroca et al., 2016). It has also been reported that exosomes containing retinal proteins were found in abundance in the vitreous humor of the mouse and human, demonstrating a level of communication that exists between these ocular tissues (Zhao et al., 2018). While it has yet to be discovered if there is any differential change in exosome composition or concentration in the vitreous during retinal degenerative diseases, exosomes identified in the aqueous humor of AMD patients were found to contain a cross-over set of proteins also found in the culture medium of aRPE19 cells (Kang et al., 2014). This finding, while largely correlative, suggests that exosomes derived from the RPE may play a role in disease pathogenesis. Furthermore, these results demonstrate the possibility that access to exosome populations in biological fluids of the eye could provide a representation of what may be occurring in the retina and therefore serves a diagnostic potential.

Exosome based gene therapies are at the forefront of therapeutic development, with multiple clinical trials underway (Lener et al., 2015; Sarko and McKinney, 2017), including for the treatment of neurodegenerative diseases (Sarko and McKinney, 2017; Mead and Tomarev, 2020). However, their use for the treatment of retinal degenerations is largely in its infancy (reviewed in Mead and Tomarev, 2020). Hajrasouliha et al. (2013) provides evidence for the immunomodulatory properties of exosomes derived from cultured retinal astrocytes (Hajrasouliha et al., 2013). Using a laser induced model of choroidal neovascularization Hajrasouliha et al. (2013), demonstrated that the periocular injection of astrocytic exosomes reduced the CCL2-dependent migration of macrophages to the lesion site and attenuated angiogenesis (Hajrasouliha et al., 2013). As CCL2 has been implicated as a key chemokine in the pathogenesis of multiple retinal degenerative diseases (Newman et al., 2012; Rutar et al., 2012; Zuzic et al., 2019), and is a known target of miR-124-3p (Zuzic et al., 2019); exosome-based therapies that replenish retinal levels of this miRNA may prove efficacious as a possible therapeutic, as evidenced in other works (Chu-Tan et al., 2018). In addition, exosomes derived from microglial cells and injected into the vitreous of mice subjected to oxygen-induced retinopathy showed protective effects, reducing avascular regions in the retina, VEGF expression, and photoreceptor apoptosis, compared to controls (Xu et al., 2019). It was hypothesized by these authors that exosomal-miR-24-3p mediated this protection against hypoxia-induced cell death (Xu et al., 2019).

The combined findings of our work uncover a novel role for retinal s-mEV in both health and degeneration, unveiling a panel of s-mEV-miRNA required for retinal homeostasis, and target networks of these gene regulators comprising inflammatory, oxidative stress and cell survival pathways. As we elude to retinal health requiring optimal levels of s-mEV, and their cargo; replenishing s-mEV loads in the retina itself may prove as efficacious therapy, and will be the focus of future works. Further, both the unique s-mEV-miRNA signature and downstream target pathways open additional avenues for therapeutic development.

CONCLUSION

Results from this work suggest that s-mEV are released from photoreceptor cells to maintain retinal homeostasis. However, as a consequence of photoreceptor cell death, s-mEV secretion and/or bioavailability becomes reduced. Consequently, retinal s-mEV cargo, which contains regulatory miRNA and other molecules, are unable to regulate immune responses, subsequently contributing to progressive retinal cell death. We hypothesis that this mechanism is likely to be involved in many retinal degenerative and inflammatory diseases.

DATA AVAILABILITY STATEMENT

The datasets presented in this study can be found in online repositories. The names of the repository/repositories and accession number(s) can be found in the article/**Supplementary Material**.

ETHICS STATEMENT

The animal study was reviewed and approved by Australian National University's (ANU) Animal Experimentation Ethics Committee (AEEC).

AUTHOR CONTRIBUTIONS

YW, AC, and RN: conceptualization, investigation, and writing – original draft. YW, AC, JC-T, and RN: methodology and data analysis. YW, AC, JC-T, RA-B, US, and RN: writing – review and editing. RN: supervision and funding acquisition.

FUNDING

This work would not have been possible without the support of the National Health and Medical Research Council of Australia (NHMRC: 1127705), Retina Australia, The Gordon and Gretel Bootes Foundation, and The ANU Translational Fellowship.

ACKNOWLEDGMENTS

The authors would like to acknowledge the facilities and the scientific and technical assistance of Microscopy Australia at the Advanced Imaging Precinct, Australian National University. This microscopy facility is supported by the University and State and Federal Governments. In addition, the facilities and staff of the John Curtin School of Medical Research Biomolecular Research Facility (JCSMR, BRF, ACT, AUS).

SUPPLEMENTARY MATERIAL

The Supplementary Material for this article can be found online at: https://www.frontiersin.org/articles/10.3389/fncel.2020.00160/full#supplementary-material

REFERENCES

Abels, E. R., and Breakefield, X. O. (2016). *Introduction to Extracellular Vesicles: Biogenesis, RNA Cargo Selection, Content, Release, and Uptake*. Berlin: Springer.

Abokyi, S., To, C.-H., Lam, T. T., and Tse, D. Y. (2020). Central role of oxidative stress in age-related macular degeneration: evidence from a review of the molecular mechanisms and animal models. *Oxidat. Med. Cell. Long.* 2020:7901270.

Abusamra, A. J., Zhong, Z., Zheng, X., Li, M., Ichim, T. E., Chin, J. L., et al. (2005). Tumor exosomes expressing Fas ligand mediate CD8+ T-cell apoptosis. *Blood Cell. Mol. Dis.* 35, 169–173. doi: 10.1016/j.bcmd.2005.07.001

Alexander, M., Hu, R., Runtsch, M. C., Kagele, D. A., Mosbruger, T. L., Tolmachova, T., et al. (2015). Exosome-delivered microRNAs modulate the inflammatory response to endotoxin. *Nat. Commun.* 6:7321.

Al-Ubaidi, M. R., Hollyfield, J. G., Overbeek, P. A., and Baehr, W. (1992). Photoreceptor degeneration induced by the expression of simian virus 40 large tumor antigen in the retina of transgenic mice. *Proc. Natl. Acad. Sci. U.S.A.* 89, 1194–1198. doi: 10.1073/pnas.89.4.1194

Anel, A., Gallego-Lleyda, A., de Miguel, D., Naval, J., and Martínez-Lostao, L. (2019). Role of exosomes in the regulation of T-cell mediated immune responses and in autoimmune disease. *Cells* 8:154. doi: 10.3390/cells8020154

Antonucci, F., Turola, E., Riganti, L., Caleo, M., Gabrielli, M., Perrotta, C., et al. (2012). Microvesicles released from microglia stimulate synaptic activity via enhanced sphingolipid metabolism. *EMBO J.* 31, 1231–1240. doi: 10.1038/emboj.2011.489

Atienzar−Aroca, S., Flores−Bellver, M., Serrano−Heras, G., Martinez−Gil, N., Barcia, J. M., Aparicio, S., et al. (2016). Oxidative stress in retinal pigment epithelium cells increases exosome secretion and promotes angiogenesis in endothelial cells. *J. Cell. Mol. Med.* 20, 1457–1466. doi: 10.1111/jcmm.12834

Bartel, D. P. (2009). MicroRNAs: target recognition and regulatory functions. *Cell* 136, 215–233. doi: 10.1016/j.cell.2009.01.002

Benedikter, B. J., Weseler, A. R., Wouters, E. F. M., Savelkoul, P. H. M., Rohde, G. G. U., and Stassen, F. R. M. (2018). Redox-dependent thiol modifications: implications for the release of extracellular vesicles. *Cell. Mol. Life Sci.* 75, 2321–2337. doi: 10.1007/s00018-018-2806-z

Bhome, R., Del Vecchio, F., Lee, G.-H., Bullock, M. D., Primrose, J. N., Sayan, A. E., et al. (2018). Exosomal microRNAs (exomiRs): Small molecules with a big role in cancer. *Cancer Lett.* 420, 228–235. doi: 10.1016/j.canlet.2018.02.002

Bian, B., Zhao, C., He, X., Gong, Y., Ren, C., Ge, L., et al. (2020). Exosomes derived from neural progenitor cells preserve photoreceptors during retinal degeneration by inactivating microglia. *J. Extracell. Vesic.* 9:1748931. doi: 10.1080/20013078.2020.1748931

Bringmann, A., Grosche, A., Pannicke, T., and Reichenbach, A. (2013). GABA and Glutamate Uptake and Metabolism in Retinal Glial (Müller) Cells. *Front. Endocrinol.* 4:48–48.

Catalano, M., and O'Driscoll, L. (2020). Inhibiting extracellular vesicles formation and release: a review of EV inhibitors. *J. Extracell. Vesic.* 9:1703244. doi: 10.1080/20013078.2019.1703244

Chan, B. D., Wong, W.-Y., Lee, M. M.-L., Cho, W. C.-S., Yee, B. K., Kwan, Y. W., et al. (2019). Exosomes in inflammation and inflammatory disease. *Proteomics* 19:1800149. doi: 10.1002/pmic.201800149

Charlotte, L., Jose, M. V., Derek, M. Y., and Sean, M. D. (2016). Microvesicles and exosomes: new players in metabolic and cardiovascular disease. *J. Endocrinol.* 228, R57–R71.

Chen, E. Y., Tan, C. M., Kou, Y., Duan, Q., Wang, Z., Meirelles, G. V., et al. (2013). Enrichr: interactive and collaborative HTML5 gene list enrichment analysis tool. *BMC Bioinform.* 14:128–128.

Chen, H., Tran, J.-T. A., Brush, R. S., Saadi, A., Rahman, A. K., Yu, M., et al. (2012). *Ceramide Signaling in Retinal Degeneration. Retinal Degenerative Diseases*. Berlin: Springer, 553–558.

Christopher, A. F., Kaur, R. P., Kaur, G., Kaur, A., Gupta, V., and Bansal, P. (2016). MicroRNA therapeutics: discovering novel targets and developing specific therapy. *Perspect. Clin. Res.* 7, 68–74.

Chu-Tan, J. A., Rutar, M., Saxena, K., Aggio-Bruce, R., Essex, R. W., Valter, K., et al. (2018). MicroRNA-124 dysregulation is associated with retinal inflammation and photoreceptor death in the degenerating RetinaMicroRNA-124 dysregulation in the degenerating retina. *Investigat. Ophthalmol. Sci.* 59, 4094–4105.

Cypryk, W., Nyman, T. A., and Matikainen, S. (2018). From inflammasome to exosome—does extracellular vesicle secretion constitute an inflammasome-dependent immune response? *Front. Immunol.* 9:2188.

Desdín-Micó, G., and Mittelbrunn, M. (2017). Role of exosomes in the protection of cellular homeostasis. *Cell Adhes. Migr.* 11, 127–134. doi: 10.1080/19336918.2016.1251000

Donoso, L. A., Kim, D., Frost, A., Callahan, A., and Hageman, G. (2006). The role of inflammation in the pathogenesis of age-related macular degeneration. *Surv. Ophthalmol.* 51, 137–152. doi: 10.1016/j.survophthal.2005.12.001

Erik, C. S. S.-M. (2017). *ggbeeswarm: Categorical Scatter (Violin Point) Plots*. Available online at: https://github.com/eclarke/ggbeeswarm (Augest 7, 2017).

Essandoh, K., Yang, L., Wang, X., Huang, W., Qin, D., Hao, J., et al. (2015). Blockade of exosome generation with GW4869 dampens the sepsis-induced inflammation and cardiac dysfunction. *Biochim. Biophys. Acta* 1852, 2362–2371. doi: 10.1016/j.bbadis.2015.08.010

Fan, Y., Siklenka, K., Arora, S. K., Ribeiro, P., Kimmins, S., and Xia, J. (2016). miRNet - dissecting miRNA-target interactions and functional associations through network-based visual analysis. *Nucleic Acids Res.* 44, W135–W141.

Fauré, J., Lachenal, G., Court, M., Hirrlinger, J., Chatellard-Causse, C., Blot, B., et al. (2006). Exosomes are released by cultured cortical neurones. *Mol. Cell. Neurosci.* 31, 642–648. doi: 10.1016/j.mcn.2005.12.003

Fernando, N., Wooff, Y., Aggio-Bruce, R., Chu-Tan, J. A., Jiao, H., Dietrich, C., et al. (2018). Photoreceptor survival is regulated by GSTO1-1 in the degenerating retina. *Investigat. Ophthalmol. Vis. Sci.* 59, 4362–4374.

Fleshner, M., and Crane, C. R. (2017). Exosomes, DAMPs and miRNA: features of stress physiology and immune homeostasis. *Trends Immunol.* 38, 768–776. doi: 10.1016/j.it.2017.08.002

Fröhlich, D., Kuo, W. P., Frühbeis, C., Sun, J.-J., Zehendner, C. M., Luhmann, H. J., et al. (2014). Multifaceted effects of oligodendroglial exosomes on neurons: impact on neuronal firing rate, signal transduction and gene regulation. *Philos. Transact. R. Soc. Lond. Ser. Biol. Sci.* 369:20130510. doi: 10.1098/rstb.2013.0510

Frühbeis, C., Fröhlich, D., Kuo, W. P., Amphornrat, J., Thilemann, S., Saab, A. S., et al. (2013). Neurotransmitter-triggered transfer of exosomes mediates oligodendrocyte–neuron communication. *PLoS Biol.* 11:e1001604. doi: 10.1371/journal.pbio.1001604

Gargini, C., Terzibasi, E., Mazzoni, F., and Strettoi, E. (2007). Retinal organization in the retinal degeneration 10 (rd10) mutant mouse: a morphological and ERG study. *J. Compar. Neurol.* 500, 222–238. doi: 10.1002/cne.21144

German, O. L., Miranda, G. E., Abrahan, C. E., and Rotstein, N. P. (2006). Ceramide is a mediator of apoptosis in retina photoreceptors. *Investigat. Ophthalmol. Vis. Sci.* 47, 1658–1668.

Gerritzen, M. J. H., Martens, D. E., Wijffels, R. H., and Stork, M. (2017). High throughput nanoparticle tracking analysis for monitoring outer membrane vesicle production. *J. Extracell. Ves.* 6:1333883. doi: 10.1080/20013078.2017.1333883

Gupta, A., and Pulliam, L. (2014). Exosomes as mediators of neuroinflammation. *J. Neuroinflam.* 11, 68–68.

Hajrasouliha, A. R., Jiang, G., Lu, Q., Lu, H., Kaplan, H. J., Zhang, H.-G., et al. (2013). Exosomes from retinal astrocytes contain antiangiogenic components that inhibit laser-induced choroidal neovascularization. *J. Biol. Chem.* 288, 28058–28067. doi: 10.1074/jbc.m113.470765

Hessvik, N. P., and Llorente, A. (2018). Current knowledge on exosome biogenesis and release. *Cell. Mol. Life Sci.* 75, 193–208. doi: 10.1007/s00018-017-2595-9

Hsu, M.-Y., Chiu, C.-C., Wang, J.-Y., Huang, C.-T., Huang, Y.-F., Liou, J.-C., et al. (2018). Paper-based microfluidic platforms for understanding the role of exosomes in the pathogenesis of major blindness-threatening diseases. *Nanomaterials (Basel Switzerland)* 8:310. doi: 10.3390/nano8050310

Huang, C., Fisher, K. P., Hammer, S. S., Navitskaya, S., Blanchard, G. J., and Busik, J. V. (2018). Plasma exosomes contribute to microvascular damage in diabetic retinopathy by activating the classical complement pathway. *Diabetes* 67, 1639–1649. doi: 10.2337/db17-1587

Isola, L., and Chen, S. (2017). Exosomes: the messengers of health and disease. *Curr. Neuropharmacol.* 15, 157–165. doi: 10.2174/1570159x14666160825160421

Jain, G., Stuendl, A., Rao, P., Berulava, T., Pena Centeno, T., Kaurani, L., et al. (2019). A combined miRNA–piRNA signature to detect Alzheimer's disease. *Transl. Psychiatry* 9:250.

Jan, A. T., Malik, M. A., Rahman, S., Yeo, H. R., Lee, E. J., Abdullah, T. S., et al. (2017). Perspective insights of exosomes in neurodegenerative diseases: a critical appraisal. *Front. Aging Neurosci.* 9:317–317.

Janik-Papis, K., Ulińska, M., Krzyzanowska, A., Stoczyńska, E., Borucka, A., Woźniak, K., et al. (2009). Role of oxidative mechanisms in the pathogenesis of age-related macular degeneration. *Klinika Oczna* 111, 168–173.

Jiao, H., Rutar, M., Fernando, N., Yednock, T., Sankaranarayanan, S., Aggio-Bruce, R., et al. (2018). Subretinal macrophages produce classical complement activator C1q leading to the progression of focal retinal degeneration. *Mol. Neurodegener.* 13:45.

Jung, M. K., and Mun, J. Y. (2018). Sample preparation and imaging of exosomes by transmission electron microscopy. *J. Vis. Exp. JoVE* 131:56482.

Kang, G.-Y., Bang, J. Y., Choi, A. J., Yoon, J., Lee, W.-C., Choi, S., et al. (2014). Exosomal proteins in the aqueous humor as novel biomarkers in patients with neovascular age-related macular degeneration. *J. Prot. Res.* 13, 581–595. doi: 10.1021/pr400751k

Kauppinen, A., Paterno, J. J., Blasiak, J., Salminen, A., and Kaarniranta, K. (2016). Inflammation and its role in age-related macular degeneration. *Cell. Mol. Life Sci. CMLS* 73, 1765–1786.

Kim, S. R., Fishkin, N., Kong, J., Nakanishi, K., Allikmets, R., and Sparrow, J. R. (2004). Rpe65 Leu450Met variant is associated with reduced levels of the retinal pigment epithelium lipofuscin fluorophores A2E and iso-A2E. *Proc. Natl. Acad. Sci. U.S.A.* 101, 11668–11672. doi: 10.1073/pnas.0403499101

Klingeborn, M., Dismuke, W. M., Rickman, C. B., and Stamer, W. D. (2017). Roles of exosomes in the normal and diseased eye. *Prog. Retin. Eye Res.* 59, 158–177. doi: 10.1016/j.preteyeres.2017.04.004

Knickelbein, J. E., Chan, C.-C., Sen, H. N., Ferris, F. L., and Nussenblatt, R. B. (2015). Inflammatory mechanisms of age-related macular degeneration. *Int. Ophthalmol. Clin.* 55:63.

Kosaka, N., Iguchi, H., Hagiwara, K., Yoshioka, Y., Takeshita, F., and Ochiya, T. (2013). Neutral sphingomyelinase 2 (nSMase2)-dependent exosomal transfer of angiogenic microRNAs regulate cancer cell metastasis. *J. Biol. Chem.* 288, 10849–10859. doi: 10.1074/jbc.m112.446831

Kowal, J., Tkach, M., and Théry, C. (2014). Biogenesis and secretion of exosomes. *Curr. Opin. Cell Biol.* 29, 116–125. doi: 10.1016/j.ceb.2014.05.004

Krol, J., Busskamp, V., Markiewicz, I., Stadler, M. B., Ribi, S., Richter, J., et al. (2010). Characterizing light-regulated retinal MicroRNAs reveals rapid turnover as a common property of neuronal MicroRNAs. *Cell* 141, 618–631. doi: 10.1016/j.cell.2010.03.039

Kyosseva, S. V. (2016). Targeting MAPK signaling in age-related macular degeneration. *Ophthalmol. Eye Dis.* 8, 23–30.

Lachenal, G., Pernet-Gallay, K., Chivet, M., Hemming, F. J., Belly, A., Bodon, G., et al. (2011). Release of exosomes from differentiated neurons and its regulation by synaptic glutamatergic activity. *Mol. Cell. Neurosci.* 46, 409–418. doi: 10.1016/j.mcn.2010.11.004

Lehmann, B. D., Paine, M. S., Brooks, A. M., McCubrey, J. A., Renegar, R. H., Wang, R., et al. (2008). Senescence-associated exosome release from human prostate cancer cells. *Cancer Res.* 68:7864. doi: 10.1158/0008-5472.can-07-6538

Lener, T., Gimona, M., Aigner, L., Börger, V., Buzas, E., Camussi, G., et al. (2015). Applying extracellular vesicles based therapeutics in clinical trials–an ISEV position paper. *J. Extracell. Ves.* 4:30087.

Li, J. J., Wang, B., Kodali, M. C., Chen, C., Kim, E., Patters, B. J., et al. (2018). In vivo evidence for the contribution of peripheral circulating inflammatory exosomes to neuroinflammation. *J. Neuroinflam.* 15:8.

Li, N., Zhao, L., Wei, Y., Ea, V. L., Nian, H., and Wei, R. (2019). Recent advances of exosomes in immune-mediated eye diseases. *Stem Cell Res. Ther.* 10:278.

Long, H., Wang, X., Chen, Y., Wang, L., Zhao, M., and Lu, Q. (2018). Dysregulation of microRNAs in autoimmune diseases: pathogenesis, biomarkers and potential therapeutic targets. *Cancer Lett.* 428, 90–103. doi: 10.1016/j.canlet.2018.04.016

Lu, Y.-Z., Fernando, N., Natoli, R., Madigan, M., and Valter, K. (2018). 670nm light treatment following retinal injury modulates Müller cell gliosis: Evidence from in vivo and in vitro stress models. *Exp. Eye Res.* 169, 1–12. doi: 10.1016/j.exer.2018.01.011

Lu, Y.-Z., Natoli, R., Madigan, M., Fernando, N., Saxena, K., Aggio-Bruce, R., et al. (2017). Photobiomodulation with 670 nm light ameliorates Müller cell-mediated activation of microglia and macrophages in retinal degeneration. *Exp. Eye Res.* 165, 78–89. doi: 10.1016/j.exer.2017.09.002

Luberto, C., Hassler, D. F., Signorelli, P., Okamoto, Y., Sawai, H., Boros, E., et al. (2002). Inhibition of tumor necrosis factor-induced cell death in MCF7 by a novel inhibitor of neutral sphingomyelinase. *J. Biol. Chem.* 277, 41128–41139. doi: 10.1074/jbc.m206747200

Marc, R. E., Jones, B., Watt, C., Vazquez-Chona, F., Vaughan, D., and Organisciak, D. (2008). Extreme retinal remodeling triggered by light damage: implications for age related macular degeneration. *Mol. Vis.* 14:782.

Mathieu, M., Martin-Jaular, L., Lavieu, G., and Théry, C. (2019). Specificities of secretion and uptake of exosomes and other extracellular vesicles for cell-to-cell communication. *Nat. Cell Biol.* 21, 9–17. doi: 10.1038/s41556-018-0250-9

Mattapallil, M. J., Wawrousek, E. F., Chan, C.-C., Zhao, H., Roychoudhury, J., Ferguson, T. A., et al. (2012). The Rd8 mutation of the Crb1 gene is present in vendor lines of C57BL/6N mice and embryonic stem cells, and confounds ocular induced mutant phenotypes. *Investigat. Ophthalmol. Vis. Sci.* 53, 2921–2927.

Mead, B., and Tomarev, S. (2020). Extracellular vesicle therapy for retinal diseases. *Prog. Retin. Eye Res.* 10:100849. doi: 10.1016/j.preteyeres.2020.100849

Men, Y., Yelick, J., Jin, S., Tian, Y., Chiang, M. S. R., Higashimori, H., et al. (2019). Exosome reporter mice reveal the involvement of exosomes in mediating neuron to astroglia communication in the CNS. *Nat. Commun.* 10:4136.

Natoli, R., Fernando, N., Madigan, M., Chu-Tan, J. A., Valter, K., Provis, J., et al. (2017). Microglia-derived IL-1β promotes chemokine expression by Müller cells and RPE in focal retinal degeneration. *Mol. Neurodegen.* 12:31.

Natoli, R., Jiao, H., Barnett, N. L., Fernando, N., Valter, K., Provis, J. M., et al. (2016). A model of progressive photo-oxidative degeneration and inflammation in the pigmented C57BL/6J mouse retina. *Exp. Eye Res.* 147, 114–127. doi: 10.1016/j.exer.2016.04.015

Natoli, R., Zhu, Y., Valter, K., Bisti, S., Eells, J., and Stone, J. (2010). Gene and noncoding RNA regulation underlying photoreceptor protection: microarray study of dietary antioxidant saffron and photobiomodulation in rat retina. *Mol. Vis.* 16:1801.

Newman, A. M., Gallo, N. B., Hancox, L. S., Miller, N. J., Radeke, C. M., and Maloney, M. A. (2012). Systems-level analysis of age-related macular degeneration reveals global biomarkers and phenotype-specific functional networks. *Genome Med.* 4:16. doi: 10.1186/gm315

Pascua-Maestro, R., González, E., Lillo, C., Ganfornina, M. D., Falcón-Pérez, J. M., and Sanchez, D. (2018). Extracellular vesicles secreted by astroglial cells transport apolipoprotein D to neurons and mediate neuronal survival upon oxidative stress. *Front. Cell Neurosci.* 12:526.

Piñero, J. À, Bravo, N., Queralt-Rosinach, A., Gutiérrez-Sacristán, J., Deu-Pons, E., Centeno, J., et al. (2016). DisGeNET: a comprehensive platform integrating information on human disease-associated genes and variants. *Nucleic Acids Res.* 45, D833–D839.

R Core Team (2019). *R: A Language and Environment for Statistical Computing*. Vienna: R Core Team.

Ratnapriya, R., and Swaroop, A. (2013). Genetic architecture of retinal and macular degenerative diseases: the promise and challenges of next-generation sequencing. *Genome Med.* 5:84.

Rivera, J. C., Holm, M., Austeng, D., Morken, T. S., Zhou, T. E., Beaudry-Richard, A., et al. (2017). Retinopathy of prematurity: inflammation, choroidal degeneration, and novel promising therapeutic strategies. *J. Neuroinflam.* 14, 165–165.

Robbins, P. D., and Morelli, A. E. (2014). Regulation of immune responses by extracellular vesicles. *Nature Rev. Immunol.* 14, 195–208. doi: 10.1038/nri3622

Rübsam, A., Parikh, S., and Fort, P. E. (2018). Role of inflammation in diabetic retinopathy. *Int. J. Mol. Sci.* 19:942. doi: 10.3390/ijms19040942

Rupaimoole, R., and Slack, F. J. (2017). MicroRNA therapeutics: towards a new era for the management of cancer and other diseases. *Nat. Rev. Drug Discov.* 16:203. doi: 10.1038/nrd.2016.246

Rutar, M., Natoli, R., Chia, R., Valter, K., and Provis, J. M. (2015). Chemokine-mediated inflammation in the degenerating retina is coordinated by Müller cells, activated microglia, and retinal pigment epithelium. *J. Neuroinflam.* 12:8. doi: 10.1186/s12974-014-0224-1

Rutar, M. V., Natoli, R. C., and Provis, J. M. (2012). Small interfering RNA-mediated suppression of Ccl2 in Muller cells attenuates microglial recruitment and photoreceptor death following retinal degeneration. *J. Neuroinflam.* 9, 5754–5760.

Sackmann, V., Sardar Sinha, M., Sackmann, C., Civitelli, L., Bergström, J., Ansell-Schultz, A., et al. (2019). Inhibition of nSMase2 reduces the transfer of oligomeric α-synuclein irrespective of hypoxia. *Front. Mol. Neurosci.* 12:200.

Saeedi, B. M. J. E., Esfandiary, G., Taheripak, P., Codoñer—Franch, E., and Mirzaei, H. (2018). Molecular aspects of diabetes mellitus: Resistin, microRNA, and exosome. *J. Cell. Biochem.* 119, 1257–1272. doi: 10.1002/jcb.26271

Sarko, D. K., and McKinney, C. E. (2017). Exosomes: origins and therapeutic potential for neurodegenerative disease. *Front. Neurosci.* 11:82.

Simón, M. V., Spalm, F. H. P., Vera, M. S., and Rotstein, N. P. (2019). Sphingolipids as emerging mediators in retina degeneration. *Front. Cell. Neurosci.* 13:246. doi: 10.3389/fncel.2019.00246

Skriner, K., Adolph, K., Jungblut, P. R., and Burmester, G. R. (2006). Association of citrullinated proteins with synovial exosomes. *Arthr. Rheum. Off. J. Am. Coll. Rheumatol.* 54, 3809–3814. doi: 10.1002/art.22276

Slenter, D. N., Kutmon, M., Hanspers, K., Riutta, A., Windsor, J., Nunes, N., et al. (2018). WikiPathways: a multifaceted pathway database bridging metabolomics to other omics research. *Nucleic Acids Res.* 46, D661–D667.

Słomka, A., Urban, S. K., Lukacs-Kornek, V., Żekanowska, E., and Kornek, M. (2018). Large extracellular vesicles: have we found the holy grail of inflammation? *Front. Immunol.* 9:2723.

Soria, F. N., Pampliega, O., Bourdenx, M., Meissner, W. G., Bezard, E., and Dehay, B. (2017). Exosomes, an unmasked culprit in neurodegenerative diseases. *Front. Neurosci.* 11:26–26.

Squadrito, M. L., Baer, C., Burdet, F., Maderna, C., Gilfillan, G. D., Lyle, R., et al. (2014). Endogenous RNAs modulate microRNA sorting to exosomes and transfer to acceptor cells. *Cell Rep.* 8, 1432–1446. doi: 10.1016/j.celrep.2014.07.035

Tam, S., Tsao, M.-S., and McPherson, J. D. (2015). Optimization of miRNA-seq data preprocessing. *Brief. Bioinform.* 16, 950–963. doi: 10.1093/bib/bbv019

Tanito, M., Kaidzu, S., Ohira, A., and Anderson, R. E. (2008). Topography of retinal damage in light-exposed albino rats. *Exp. Eye Res.* 87, 292–295. doi: 10.1016/j.exer.2008.06.002

Théry, C., Witwer, K. W., Aikawa, E., Alcaraz, M. J., Anderson, J. D., Andriantsitohaina, R., et al. (2018). Minimal information for studies of extracellular vesicles 2018 (MISEV2018): a position statement of the International Society for Extracellular Vesicles and update of the MISEV2014 guidelines. *J. Extracell. Ves.* 7:1535750.

Théry, C., Zitvogel, L., and Amigorena, S. (2002). Exosomes: composition, biogenesis and function. *Nat. Rev. Immunol.* 2:569. doi: 10.1038/nri855

Van der Pol, E., Böing, A. N., Harrison, P., Sturk, A., and Nieuwland, R. (2012). Classification, functions, and clinical relevance of extracellular vesicles. *Pharmacol. Rev.* 64, 676–705. doi: 10.1124/pr.112.005983

Van Hezel, M. E., Nieuwland, R., Van Bruggen, R., and Juffermans, N. P. (2017). The ability of extracellular vesicles to induce a pro-inflammatory host response. *Int. J. Mol. Sci.* 18:1285. doi: 10.3390/ijms18061285

Van Niel, G., Porto-Carreiro, I., Simoes, S., and Raposo, G. (2006). Exosomes: a common pathway for a specialized function. *J. Biochem.* 140, 13–21. doi: 10.1093/jb/mvj128

Vella, L. J., Scicluna, B. J., Cheng, L., Bawden, E. G., Masters, C. L., Ang, C.-S., et al. (2017). A rigorous method to enrich for exosomes from brain tissue. *J. Extracell. Vesic.* 6:1348885. doi: 10.1080/20013078.2017.1348885

Vidal-Gil, L., Sancho-Pelluz, J., Zrenner, E., Oltra, M., and Sahaboglu, A. (2019). Poly ADP ribosylation and extracellular vesicle activity in rod photoreceptor degeneration. *Sci. Rep.* 9:3758.

Wan, P., Su, W., Zhang, Y., Li, Z., Deng, C., Li, J., et al. (2019). LncRNA H19 initiates microglial pyroptosis and neuronal death in retinal ischemia/reperfusion injury. *Cell Death Differ.* 27:1.

Wang, A. L., Lukas, T. J., Yuan, M., Du, N., Tso, M. O., and Neufeld, A. H. (2009). Autophagy and exosomes in the aged retinal pigment epithelium: possible relevance to drusen formation and age-related macular degeneration. *PLoS One* 4:e4160. doi: 10.1371/journal.pone.0004160

Wang, K., Li, H., Sun, R., Liu, C., Luo, Y., Fu, S., et al. (2018). Emerging roles of transforming growth factor β signaling in wet age-related macular degeneration. *Acta Biochim. Biophys. Sinica* 51, 1–8. doi: 10.1093/abbs/gmy145

Wickham, H. (2016). *ggplot2: Elegant Graphics for Data Analysis*. New York, NY: Springer-Verlag.

Wong, W. Y., Lee, M. M. L., Chan, B. D., Kam, R. K. T., Zhang, G., Lu, A. P., et al. (2016). Proteomic profiling of dextran sulfate sodium induced acute ulcerative colitis mice serum exosomes and their immunomodulatory impact on macrophages. *Proteomics* 16, 1131–1145. doi: 10.1002/pmic.201500174

Wooff, Y., Man, S. M., Natoli, R., Aggio-Bruce, R., and Fernando, N. (2019). IL-1 Family members mediate cell death, inflammation and angiogenesis in retinal degenerative diseases. *Front. Immunol.* 10:1618.

Wu, H., Wang, C., and Wu, Z. (2013). A new shrinkage estimator for dispersion improves differential expression detection in RNA-seq data. *Biostatistics (Oxford England)* 14, 232–243. doi: 10.1093/biostatistics/kxs033

Xiang, L., Chen, X.-J., Wu, K.-C., Zhang, C.-J., Zhou, G.-H., Lv, J.-N., et al. (2017). miR-183/96 plays a pivotal regulatory role in mouse photoreceptor maturation and maintenance. *Proc. Natl. Acad. Sci. U.S.A.* 114:6376. doi: 10.1073/pnas.1618757114

Xu, W., Wu, Y., Hu, Z., Sun, L., Dou, G., Zhang, Z., et al. (2019). Exosomes from microglia attenuate photoreceptor injury and neovascularization in an animal model of retinopathy of prematurity. *Mol. Ther. Nucleic Acids* 16, 778–790. doi: 10.1016/j.omtn.2019.04.029

Yáñez-Mó, M., Siljander, P. R.-M., Andreu, Z., Bedina Zavec, A., Borràs, F. E., Buzas, E. I., et al. (2015). Biological properties of extracellular vesicles and their physiological functions. *J. Extracell. Ves.* 4:27066.

Ye, S.-B., Li, Z.-L., Luo, D.-H., Huang, B.-J., Chen, Y.-S., Zhang, X.-S., et al. (2014). Tumor-derived exosomes promote tumor progression and T-cell dysfunction through the regulation of enriched exosomal microRNAs in human nasopharyngeal carcinoma. *Oncotarget* 5, 5439. doi: 10.18632/oncotarget.2118

Yuana, Y., Sturk, A., and Nieuwland, R. (2013). Extracellular vesicles in physiological and pathological conditions. *Blood Rev.* 27, 31–39. doi: 10.1016/j.blre.2012.12.002

Zhang, H.-G., Liu, C., Su, K., Yu, S., Zhang, L., Zhang, S., et al. (2006). A membrane form of TNF-α presented by exosomes delays T cell activation-induced cell death. *J. Immunol.* 176, 7385–7393. doi: 10.4049/jimmunol.176.12.7385

Zhang, W., Ma, Y., Zhang, Y., Yang, J., He, G., and Chen, S. (2019). Photo-oxidative blue-light stimulation in retinal pigment epithelium cells promotes exosome secretion and increases the activity of the NLRP3 inflammasome. *Curr. Eye Res.* 44, 67–75. doi: 10.1080/02713683.2018.1518458

Zhao, Y., Weber, S. R., Lease, J., Russo, M., Siedlecki, C. A., Xu, L.-C., et al. (2018). Liquid biopsy of vitreous reveals an abundant vesicle population consistent with the size and morphology of exosomes. *Transl. Vis. Sci. Technol.* 7, 6–6.

Ziemann, M., Kaspi, A., and El-Osta, A. (2016). Evaluation of microRNA alignment techniques. *RNA* 22, 1120–1138. doi: 10.1261/rna.055509.115

Zuzic, M., Rojo, A. J. E., Wohl, S. G., and Busskamp, V. (2019). Retinal miRNA functions in health and disease. *Genes* 10:377. doi: 10.3390/genes10050377

Conflict of Interest: The authors declare that the research was conducted in the absence of any commercial or financial relationships that could be construed as a potential conflict of interest.